Energy Conversion and Management 213 (2020) 112852

Contents lists available at ScienceDirect

Energy Conversion and Management

journal homepage: www.elsevier.com/locate/enconman

Annual thermoeconomic analysis of a Concentrating Solar Power + Photovoltaic + Multi-Effect Distillation plant in northern Chile

Carlos Mata-Torres[a,*], Patricia Palenzuela[b], Adriana Zurita[a], José M. Cardemil[c], Diego-César Alarcón-Padilla[b], Rodrigo A. Escobar[a,d]

[a] Departamento de Ingeniería Mecánica y Metalúrgica, Escuela de Ingeniería, Pontificia Universidad Católica de Chile, Vicuña Mackenna 4860, Santiago, Chile
[b] CIEMAT – Plataforma Solar de Almeria, Ctra. de Senés s/n, 04200 Tabernas, Almería, Spain
[c] Departamento de Ingeniería Mecánica, Facultad de Ciencias Físicas y Matemáticas, Universidad de Chile, Beauchef 851, Santiago, Chile
[d] Centro del Desierto de Atacama, Escuela de Ingeniería. Pontificia Universidad Católica de Chile, Vicuña Mackenna 4860, Santiago, Chile

ARTICLE INFO

Keywords:
Thermoeconomic analysis
CSP + D
CSP + PV + MED
Cogeneration plant
Chile

ABSTRACT

A detailed annual performance and thermoeconomic analysis of a Concentrated Solar Power plant coupled to a Photovoltaic and a Multi-Effect Distillation plants (CSP + PV + MED) were performed using an extensive methodology based on an hourly simulation. The aim was to assess the impact of the PV integration into the CSP + PV plant and to evaluate the sizing of the plant in terms of the design parameters (PV plant size, solar multiple, Thermal Energy Storage capacity, and numbers of MED units) that allow achieving the lowest thermoeconomic electric and water costs (TCE and TCW). Results show that PV integration mainly increases the electric output but could increase the water production depending on the PV and CSP plants' sizes. Moreover, the PV plant cost is mainly allocated to electricity, decreasing the TCE, while on the TCW it has a moderate impact. Finally, it was found that the PV plant and the CSP plant size has contradictory roles between the costs, where the minimum TCE is obtained for large PV plant with an undersized CSP plant and one MED unit, and the minimum TCW is obtained for small PV plant with an oversized CSP plant and a large MED plant (5 units).

1. Introduction

A growing interest in desalination technologies has been evidenced in the last years in response to a rising demand and water shortage worldwide, which has led to an increase of the global installed capacity of this type of technologies [1,2]. Within the desalination market, Reverse Osmosis (RO) is the dominating technology with more than 67% of worldwide installed capacity, followed by thermal desalination [1,3,4]. The growing freshwater demand has also led to an increase in the energy demand and consumption rate of fossil fuels since desalination systems are processes with high energy intensity that are associated with conventional thermoelectric power plants. Therefore, future development of desalination plants using sustainable energy sources is being considered as an opportunity, where renewables energies represent one of the most relevant solutions [5].

Northern Chile has become a case study because it is one of the aridest regions worldwide, and it also constitutes the area where the most relevant mining facilities of the country are located. Water supply in this region is mainly obtained from aquafers that have been overexploited over the last years, leading mining industries to start looking for new sources of freshwater, such as desalination plants [6]. In this way, water for mining coming from desalination has been progressively increasing in the course of the last years, and it is expected to be triplicated by 2029 [7,8]. Besides this, most of the demand spots are located inland between 1000 and 4000 m above the sea level, which makes the water conveyance (pipeline cost and pumping) an essential aspect of these systems [9]. Water cost in Chile ranges from 1.4 to 5.5 $\$/m^3$, where water conveyance represents approximately 40–90% of the total cost [10]. On the other hand, northern Chile is endowed with one of the highest levels of solar irradiation in the world due to a combination of meteorological and geographical conditions, reaching Direct Normal Irradiation (DNI) levels up to 3500 kWh/m^2-yr [11,12]. Thus, the integration of Concentrating Solar Power and Desalination (CSP + D) systems have been proposed as case studies in this region due to its possible potential.

The Concentrating Solar Power (CSP) plants constitute a natural partner for thermal desalination [3], with the potential of reducing environmental impact and solving the freshwater supply issue in remote areas, however, the integration of CSP + D plants has not been demonstrated in a commercial project yet [13]. Among the vast

* Corresponding author.
E-mail address: cnmata@uc.cl (C. Mata-Torres).

https://doi.org/10.1016/j.enconman.2020.112852
Received 24 January 2020; Received in revised form 8 April 2020; Accepted 10 April 2020
Available online 22 April 2020

literature on this topic, Mohammadi et al. [14] presented a detailed and extensive review of the state-of-the-art of CSP + D systems focused on only freshwater and cogenerating plants (electricity and freshwater), in which the potential of these systems is described, highlighting the integration with Multi-Effect Distillation (MED) systems. However, it is also recognized that the main commercial barriers for these systems are the solar field cost, the integration strategy, and the conservative behavior of the desalination market [4,13].

Regarding CSP + MED systems, several studies have been conducted assessing their performance [15–18], and the results have shown that CSP + MED could be competitive against RO under specific conditions of the location. In this context, Sharan et al. [19] analyzed a CSP + MED concept in which a supercritical CO_2 power cycle was integrated to a MED plant and the evaluation was conducted in six coastal locations, obtaining competitive and even lower water costs than a RO plant. Additionally, some authors have performed analyses considering the effect of the distance from the sea and the altitude of the location [20,21], demonstrating that the seawater pumping system represents a significant contribution to the water cost. Therefore, the study of such systems should consider the impact of geographical conditions such as DNI levels, location's altitude and distance from the coast, as well as the water salinity.

Another concept that has been studied is the hybridization of a CSP with a Photovoltaic (PV) plant, which combines the benefit of the low cost of a PV plant, with the flexible dispatchability of a CSP plant to increase its capacity factor. Thus, several optimal configurations that allow integrating the production of both plants have been identified by different authors [22,23]. However, the hybridization of a CSP + MED plant with a PV system presents different outcomes. According to Valenzuela et al. [24], the hybridization allows reducing the electricity and the water costs but enforces the CSP + MED plant to operate at part-load several hours throughout the year.

These studies have mainly performed economic analyses based on energy, known as levelized cost methodology, which allows determining the cost of the products of a system. Nonetheless, the thermoeconomic method is a more accurate option to analyze complex cogeneration plants that would enable obtaining an appropriate assessment of the cost of the products, i.e. electricity and water, as it integrates an exergy analysis with an economic analysis [25,26]. In the literature, several authors have evaluated the thermoeconomic cost of a combined power and heat (CPH) plant or CSP plant integrated with MED plant for electricity and water production [27–29], identifying that the best design recommendation is to use lower steam extraction pressure and replacing the condenser by a MED plant. However, it is also essential to reduce the investment cost of the system for achieving economic viability.

These thermoeconomic analyses are focused on the plant's design and configuration, but the integration of a PV plant to a CSP + MED implies that the plant would operate at different off-design conditions, and the variability of the solar irradiation must be considered. In addition to that, the location of the plant with respect to the sea level, as well as of the pumping system costs, must be assessed because they can drastically change the yield and the cost of the products. In a previous study developed by the authors [30], a thermoeconomic analysis of a Rankine Cycle integrated to a MED plant was performed, evaluating the impact of the part-load operation, ambient temperature, MED plant size, and location's altitude on its performance. The results showed that the component costs have a higher impact on the product costs than the destroyed and waste exergy, pointing out that the part-load operation significantly impacts both costs. Larger MED plants achieved the lowest cost of electricity and water, while the locations' altitude increased the cost of the water significantly. This analysis exposes the impact of operational conditions on the performance of the plant, but it is required to include the CSP components operation and cost, and the solar irradiation variability, to properly assess their impact on the product costs formation. Lastly, Mata-Torres et al. [31] performed an analysis of a CSP + PV + MED plant evidencing that PV integration mainly increases the electricity output and moderately increases the water production while the thermoeconomic costs of the products decrease, especially the electricity cost. However, this analysis considers only one scenario in which the cost of the P/R system was not considered. Thus, there is a lack of information on assessing the actual impact of the integration of the PV plant to a CSP + MED, and how these systems can work in a cogeneration scheme, as well as determining the size of the system that deliver the lower costs.

This study presents the annual performance and thermoeconomic analysis of a CSP + PV + MED plant located in northern Chile. The goal is to assess the benefits and drawbacks of the integration of a PV plant into the CSP + MED plant. For this purpose, the performance and the process of cost formation on this system integration have been analyzed. The analysis has been carried out by applying an extensive methodology based on an hourly simulation of the plant and an hourly thermoeconomic analysis that allows calculating the daily, monthly, and annual costs. The cost allocation of the systems to the products (electricity and water) has also been assessed considering the hourly variation of the irradiation data and their effect on the operation of the plant. A unidimensional analysis in terms of the design parameters of the plant (size of the PV plant, solar multiple, Thermal Energy Storage capacity, and the number of MED units) has been carried out in order to analyze the impact of these parameters on the plant performance and products costs. Finally, a multivariable parametric analysis varying the design parameters of the plant was carried out to find the configuration that allows obtaining the lowest costs of electricity and water. Therefore, the detailed thermoeconomic analysis presented herein allows assessing the actual production costs of a CSP + PV + MED plant considering the annual operation for a specific location and exposes the impact of the design parameters on the operation costs of the plant.

2. System description

The system consists of a MED unit integrated to a CSP + PV plant, in a schemed called as CSP + PV + MED plant. Fig. 1 shows the layout of the plant with further details of the components, systems, and subsystems considered. As observed in the figure, the MED unit is coupled with the power block of the CSP plant in parallel to the condenser. Also, a seawater pumping system to feed the MED plant, and a system that recovers the potential energy of the resultant brine disposal returned to the sea (P/R system) is considered. The plant operates delivering a net power output of 100 MW_e to the grid. In order to fulfill this objective, the PV plant has been established as the priority to deliver the electric power to the grid, and the CSP plant works as a backup [22,24,32]. This operation strategy would allow storing thermal energy in the Thermal Energy Storage (TES) system to be used in periods of low irradiation that, in turn, would increase the net output power of the whole plant. Notice that the parasitic consumption of the plant (from the solar tower, the power block, the MED plant, and the seawater pumping system) is also included in the electric power balance.

2.1. CSP plant

The CSP plant consists of a central receiver tower plant with a two-tank direct TES system, and a steam power block with a gross output power of 110 MW_e. The plant uses a molten salt mixture (60% $NaNO_3$ and 40% KNO_3) as heat transfer fluid (HTF) and storage media. The central receiver consists of a cylindrical receiver that heats the HTF up to 565 °C [33]. Then, the molten salts are stored in the hot tank. As required the hot salts flow through the Steam Generation System (SGS) delivering heat to a power block that produces electricity in a steam turbine. The cold molten salts are stored in the cold tank around 300 °C. The solar field is composed of heliostats with an area of 144 $m^{2,}$ having a reflectivity of 95% [34]. The power block consists of a steam Rankine Cycle, which considers a high-pressure turbine stage, a low-pressure

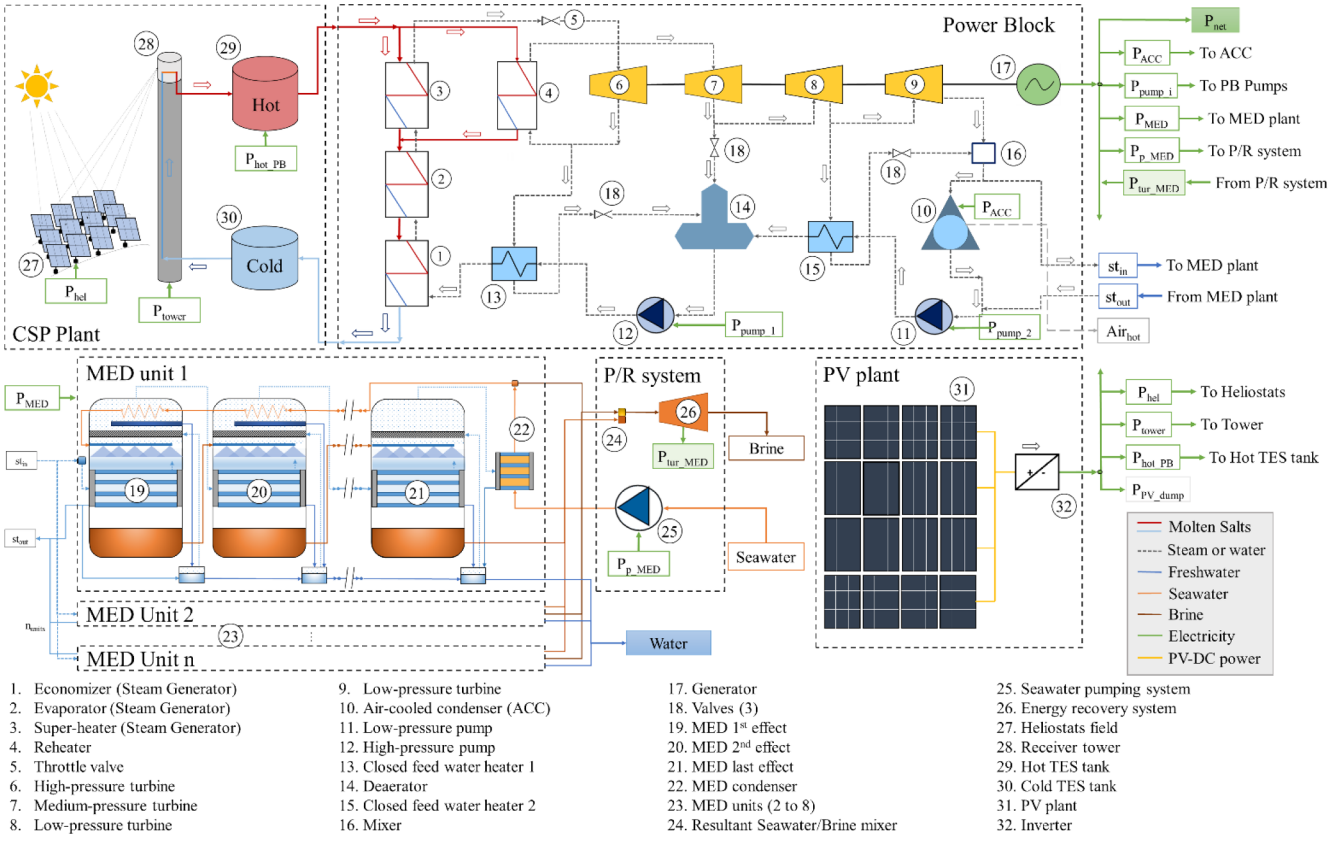

1. Economizer (Steam Generator)
2. Evaporator (Steam Generator)
3. Super-heater (Steam Generator)
4. Reheater
5. Throttle valve
6. High-pressure turbine
7. Medium-pressure turbine
8. Low-pressure turbine
9. Low-pressure turbine
10. Air-cooled condenser (ACC)
11. Low-pressure pump
12. High-pressure pump
13. Closed feed water heater 1
14. Deaerator
15. Closed feed water heater 2
16. Mixer
17. Generator
18. Valves (3)
19. MED 1st effect
20. MED 2nd effect
21. MED last effect
22. MED condenser
23. MED units (2 to 8)
24. Resultant Seawater/Brine mixer
25. Seawater pumping system
26. Energy recovery system
27. Heliostats field
28. Receiver tower
29. Hot TES tank
30. Cold TES tank
31. PV plant
32. Inverter

Fig. 1. Scheme of the CSP + PV + MED plant proposed.

turbine stage with three extractions, two Close Feed-Water Heaters (CFWH), a deaerator, a reheater and an Air Cooled-Condenser (ACC). The steam can be condensed by a MED plant coupled at the turbine exhaust steam outlet, in parallel to the ACC. In this configuration, the turbine back pressure is set to the saturation temperature of the MED plant inlet steam.

2.2. PV plant

The PV plant consists of a modular PV plant with one-axis tracking and inverters of 1 MW_e. The PV plant size is scalable with the number of inverters and is connected in parallel with the power block. In this way, the PV plant and the power block work in synergy to deliver a baseload capacity.

2.3. MED plant and P/R system

The MED plant consists of several units of 10,000 m^3/day capacity each, with a forward-feed plant configuration of 14 effects and 13 pre-heaters. The design parameters of the MED unit are as follows: the steam enters at the first effect at 70 °C, the seawater inlet temperature is 20 °C, and the salinity is 35 g_{salt}/kg_{water}. The temperature of the last effect is 34 °C, while the brine output salinity is 63 g_{salt}/kg_{water}. With these parameters, each unit requires a steam mass flow rate of 11.45 kg/s or 25.9 MW_{th} of thermal energy to reach the nominal operating conditions. Considering that the maximum exhaust steam mass flow rate of the power block is 88 kg/s at nominal conditions, the maximum number of units of the MED plant would be 8. Moreover, if another salinity is considered due to being in another location, the MED plant design parameters (number of effects and steam mass flow rate) and performance would change. Finally, the P/R system considers two pipelines, one for the seawater pumped and another for the brine disposal. In addition, it is considered a seawater pumping station, and a hydraulic turbine.

3. Model development

The simulation model for the CSP + PV + MED plant was developed in Transient System Simulation Program (TRNSYS) software, which was also used to run the simulations with the aim of determining the performance of each system, subsystem, and components of the plant. The model was developed in a single TRNSYS deck that integrates the electric power balance between the different components of the plant, as well as the startup and shut down of these components. Most of the TRNSYS types were developed by the authors in previous works [22,30]. The simulations were performed for a Typical Meteorological Year (TMY) with data on an hourly basis.

3.1. CSP and PV plant

The CSP plant model is composed of the heliostats, the central receiver, and the thermal storage tank types [20,22,24]. The TRNSYS Type that describes the heliostats field was developed based on Type 394 from the STEC (Solar Thermal Electric Components) library [35], which establishes a heliostats field efficiency in function of the solar altitude and azimuth to calculate the incident power on the receiver. This model considers a power consumption of the heliostats, a daily soling rate, and a cleaning period of 0.055 kW_e, 0.5%, and 20 days, respectively [22,36].

The central receiver type is a simplified model of a cylindrical receiver composed by tubes. The model calculates the HTF mass flow rate at a defined outlet temperature in terms of the incident radiation, the thermal losses, and the input HTF temperature. The thermal losses are constituted by the natural and forced convection losses and the radiation losses, which depends on the wind velocity, the ambient and sky temperatures, the central receiver and tower dimensions, and receiver

superficial temperature. Also, the model considers the electric power consumption of the HTF tower pumps according to the HTF mass flow rate flowing through the receiver. The design of the receiver and of the heliostats solar field were calculated in terms of the solar multiple (SM - rate between the solar field thermal power and the thermal power of the power block at the nominal point) using SAM from NREL [34,36]. Moreover, the central receiver integrates a control procedure that delimits its operation by four parameters controls:

1. Energy required to start up the tower operation, set to 25% of the nominal thermal energy for 1 h.
2. Minimum thermal power to initiate the startup, set to 20% of the nominal power,
3. Minimum thermal power to operate the receiver in normal conditions, set to 25% of the nominal thermal power.
4. Maximum thermal power operation defined at 110% of the nominal power.

The TES system was modeled considering two storage tanks with variable volume (Type 39 from TRNSYS library), one for the hot HTF tank, and another for the cold HTF tank. A control system was integrated into the TES model, in which the HTF mass flow rate that goes to the power block was restricted in terms of the hot tank volume in order to decrease the number of the power block start-ups, allowing the power block operation for at least two hours [22]. The electric power consumption related to the power block HTF pumps was also considered in this model.

Lastly, the PV plant was simulated using the Type 190 of TRNSYS, which includes the inverter efficiency curve and determines the electrical performance of the PV array. The size of the array was set to 1 MW_e (20 modules in series and 178 strings in parallel) and was scaled up to the PV plant size in terms of the number of inverters. In this analysis, it was considered a one-axis tracking to maximize the yearly yield of the plant, and an average soiling rate of 10%.

3.2. Power block

The power block model, used in a previous work by the authors [30], was developed in Engineering Equation Solver (EES) software to calculate the performance of the power block operating at nominal and off-design conditions. The model allows determining the design parameters of the power block, such as the overall heat transfer coefficients (UA) of the evaporator, the superheater, the reheater, and the CFWHs. The same design parameters that were used in Mata-Torres et al. [30] were considered for this study. These parameters are used as inputs for the off-design model in EES to calculate the yield of the power block. The off-design model considers a constant pressure control during part-load operation, establishing a minimum of 30% for part-load operation. The variation of the steam mass flow rate in the heat exchangers to calculate the effective UA under part-load operation (equation presented in [37]) and the change of efficiency and the pressures of the steam turbines by the Stodola's ellipse law were also considered.

The integration of the power block model into the TRNSYS environment was carried out by the use of a multi-variable polynomial regression in order to reduce the computational time significantly. The inputs of the polynomial regression were: the temperature of the HTF leaving the hot tank (T_{inHTF}), the HTF mass flow rate ($\dot{m}_{inHTF}$) and the condensing temperature (T_s). Notice that the condensing temperature (that is, in turn, the steam temperature at the inlet of the MED first effect) is established by the part-load operation of the MED unit (see Section 3.3). The outputs of the regression were: the net power output from the turbine-generator (W_{net}), the turbine exhaust mass flow rate ($\dot{m}_{cond}$), the turbine exhaust enthalpy (h_s) and the temperature of the HTF returning to the cold tank (T_{outHTF}). The polynomial regression was obtained by performing a parametric analysis with the power block model implemented in EES, considering 11.000 operation points in a range of T_{inHTF} between 550 and 565 °C (range established according to preliminary simulations), $\dot{m}_{inHTF}$ between 200 and 700 kg/s (corresponding to off-design from 30% to 105%), and T_s between 56 and 74 °C (range established according to preliminary simulations). Once the results from the parametric analysis are determined, the tool MultiPolyRegress in MATLAB software is used to fit a polynomial regression, considering a second-degree polynomial. Finally, this regression is implemented in a TRNSYS type to estimate the yield of the power block. The Normalized Root-Mean-Square Deviation (NRMSD) of the regression model outputs was 0.25% for the W_{net}, 0.01% for the $\dot{m}_{cond}$, 0.62% for the h_s, and 0.43% for the T_{outHTF}, which proves its good accuracy. The polynomial multi-variable regression together with the coefficients used for each of the output is shown in Appendix A.1.

3.3. MED plant and P/R system

The MED unit model was implemented in EES and is based on the model proposed by Ortega-Delgado et al. [38,39] and Palenzuela et al. [40,41], already used by the authors in [30]. The model evaluates the thermodynamic performance of the MED unit by applying mass and energy balances. To model the integration of the MED unit with the rest of the plant in TRNSYS, a multi-variable polynomial regression was developed from the results delivered by the model in EES. This model was first used to determine the design condition for a 10.000 m^3/day unit, where the effects, preheaters, and the final condenser areas were calculated. Then, the part-load operation was evaluated in terms of the available thermal load in the power block and the seawater temperature considering that it changes throughout the year. The inputs of the polynomial regression were: the inlet seawater temperature (T_{sw}), the enthalpy (h_s) and the mass flow rate ($\dot{m}_s$) of the turbine's exhaust steam. Also, the temperature of the last effect of the MED unit and the output brine concentration were kept constant at their nominal values. The outputs from the polynomial regression are: the freshwater mass flow rate ($\dot{m}_{water}$), the feed seawater mass flow rate ($\dot{m}_f$), the cooling seawater mass flow rate ($\dot{m}_{csw}$), the steam temperature at the inlet of the first effect (T_s), the freshwater outlet temperature (T_{water}), the brine outlet temperature (T_{br}), and the outlet temperature of seawater at the last condenser (T_{csw}). It is important to highlight that the variation of T_s in off-design conditions is due to the decrease on the temperature difference between effects when the steam mass flow rate decreases. The regressions and their coefficients are listed in Appendix A.2.

The polynomial regression was developed by performing a parametric analysis using the MED model in EES, considering 567 operational points ranging the thermal load between 40 and 100% (which represents the variation of the inlet steam mass flow rate from 4.58 kg/s to 11.45 kg/s), the inlet steam enthalpy between 2550 and 2950 kJ/kg, and the seawater temperature between 15 and 23 °C. The regression coefficients for the seven outputs were obtained using the regression tool in MATLAB. The variation of the freshwater mass flow rate ($\dot{m}_{water}$), the total seawater mass flow rate ($\dot{m}_{in}$ - sum of the feed and cooling seawater mass flow rates), and the steam temperature at the first effect inlet (T_s), in terms of the thermal load and the seawater temperature are shown in Fig. 2.

It is observed that the freshwater mass flow rate (Fig. 2.a) and the steam saturation temperature at the inlet of the first effect (Fig. 2.c) increase significantly with the thermal load, changing from 67 to 115 kg/s; and from 60 to 70 °C, respectively. However, the variation of the seawater temperature has a negligible effect on such two variables. Regarding the total seawater mass flow rate (Fig. 2.b), it is observed that it increases dramatically with the rise of the seawater temperature at all thermal loads, showing a change from 370 kg/s to 850 kg/s at 100% of thermal load. It is worth noting that the variation of the steam temperature at the first effect inlet with the thermal load (in a range of 10 °C) would have an impact on the turbine exhaust pressure and on the power produced by the power block. Likewise, the increase of the total seawater mass flow rate with the seawater temperature would lead to

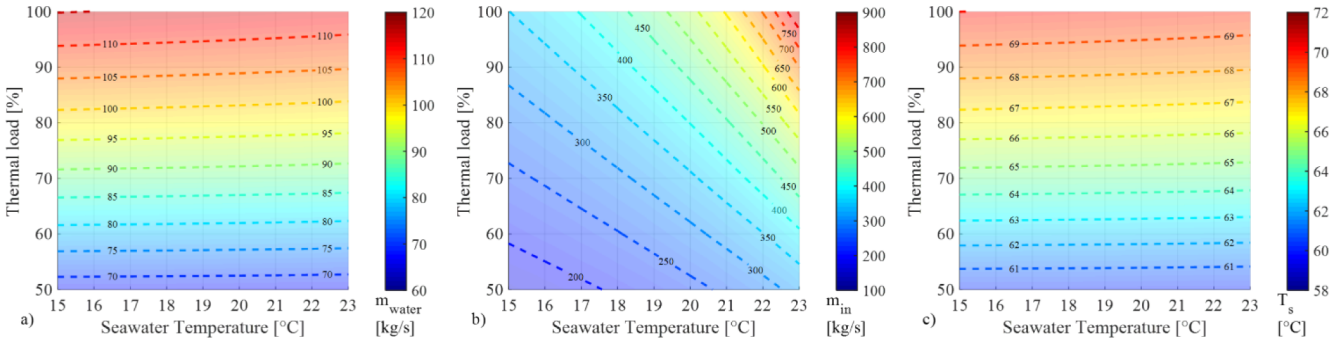

Fig. 2. (a) Freshwater mass flow rate, (b) total seawater mass flow rate, and (c) steam temperature at the inlet of the first effect variation at different thermal loads and seawater temperature.

Table 1
NRMSD of the outputs of the MED unit model.

Variable	NRMSD
Freshwater mass flow rate ($\dot{m}_{water}$)	0.16%
Feed seawater mass flow rate ($\dot{m}_f$)	0.16%
Cooling seawater mass flow rate ($\dot{m}_{csw}$)	0.71%
Steam temperature at the inlet of the first effect (T_s)	0.25%
Freshwater outlet temperature (T_{water})	0.35%
Brine outlet temperature (T_{br})	0.00%
Cooling seawater temperature (T_{csw})	0.55%

additional seawater pumping requirements for the MED cooling purposes, affecting the plant's energy consumption.

The Normalized Root-Mean-Square Deviation (NRMSD) has been used to evaluate the fit of the regression model for the seven outputs. The NRSMD results are depicted in Table 1, showing that the errors are below 1% with the highest value related to the cooling seawater mass flow rate. Therefore, the regression model developed in this work shows good accuracy and concordance with the ESS model, with the advantage of reducing significantly the computational time for the simulation.

The regression model of the MED unit was implemented in a new TRNSYS Type and integrated into the CSP + PV plant model. For this purpose, some assumptions and control procedures that limit the MED operation were considered, as follows:

1. All MED units operate at the same thermal load, which means that the steam mass flow rate that goes to the MED plant is equally divided between the MED units. Likewise, the freshwater mass flow rate obtained from the MED unit is multiplied by the number of units.
2. The maximum thermal load of the MED plant is defined in terms of the number of units and the steam mass flow rate of one unit at the design point (11.45 kg/s).
3. When the MED plant is under operation, it is powered first, and then, the remaining steam is condensed in the ACC.
4. A minimum thermal load of 70% is needed for the starting-up the MED unit in order to account the energy requirements for the start-up in the simulations.
5. When the thermal load decreases below 50%, the units are turned off, and the ACC is activated for condensing all the turbine exhaust steam.
6. The inlet steam saturation temperature obtained by the operation of the MED plant sets the condensing temperature of the power block, which varies between 60 and 70 °C according to Fig. 2.c. Moreover, when the MED plant is turned off, the condensing temperature of the power block is fixed to 60 °C.
7. The MED unit considers the specific electric consumption of 1.5 kWh/m^3 [16].

The total seawater mass flow rate pumped to the MED plant ($\dot{m}_f + \dot{m}_{csw}$), and the resultant brine mass flow rate that is returned to the sea ($\dot{m}_{csw} + \dot{m}_{br}$), were used for the evaluation of the P/R system. The assessment consists on calculating the head losses for the intake and discharge pipelines, and the power consumption of the seawater pumps and the brine recovery energy from the hydraulic turbine, considering an efficiency of 80%. The pipelines diameter was calculated as a function of the total seawater mass flow rate of the MED plant at nominal conditions and the maximum allowable inner tube velocity, which was defined at 2.5 m/s to avoid corrosion [9]. The head losses of both systems were computed using the Darcy–Weisbach equation. The friction factor was calculated in terms of the length, diameter, and the relative roughness of the pipeline, and the kinematic viscosity of the fluid. All the electrical consumptions are considered as part of the electric power balance of the plant for each time step of the simulation.

4. Thermoeconomic model

The thermoeconomic analysis is a methodology that merges the thermodynamic assessment based on the exergy and the economic analysis providing valuable information about the cost formation of the products in a cogeneration plant. The analysis was performed using a combination of procedures in EES and MATLAB softwares and using the information obtained from the thermodynamic modeling of the plant on an hourly basis. The methodology is based on a well-known process [42] that was extended on a previous work by the authors, described in [30].

4.1. Exergy analysis

The exergy analysis was applied to each energy and mass flow in the plant, considering the solar energy, molten salts, steam, seawater, freshwater, and brine streams. The analysis was performed considering a medium-disaggregation level of the systems, focusing on the power block system [30]. In detail, there were considered 88 exergy flows between the solar radiation, molten salts, steam, seawater, freshwater and brine streams, and 30 components (4 for the CSP plant, 20 for the power block, 1 for the MED plants, 3 for the P/R system, and 2 for the PV plant, presented in Fig. 1). Regarding the solar radiation, the exergy was computed considering the Petela's approach [43], using the Direct Normal Irradiation (DNI) for the heliostats and receiver components, and the Irradiation on Plane of the Array (POA) for the PV plant. Likewise, the physical exergy was calculated for the rest of the streams, while the chemical exergy was considered only for the flows related to the seawater, freshwater, and brine since in those streams the change on the salinity requires such treatment [44,45]. The physical exergy was denoted by ψ, and it is defined as:

$$\psi = (h - h_0) - T_0(s - s_0) + gz \quad (1)$$

where h and s are the enthalpy and entropy of the stream at a given

state, properties with the subscript "0" are at the reference state, g is the gravity, and z is the altitude. Potential exergy was only considered for the streams related to the MED plant and P/R system because they have a considerable change of altitude. The EES library was used for assessing the thermophysical properties of molten salts and steam, while properties of the seawater, freshwater, and brine were calculated by the correlation defined by Sharqawy et al. [46]. The chemical exergy (a_{ch}) is defined by the salinity using the approach of the chemical potential and the mass fraction, as follows:

$$a_{ch} = \sum_{i=1}^{n} w_i(\mu_i^* - \mu_i^0) \tag{2}$$

where w_i is the water or salt mass fraction (dimensionless), and μ_i is the chemical potential of the water or the salt in seawater in kJ/kg. The chemical potential of the seawater is calculated by correlations set in detail by Sharqawy et al. [47], where the μ_i^* is chemical potential at the stream salinity and the reference temperature, while the μ_i^0 is calculated considering the seawater reference salinity and temperature.

4.2. Thermoeconomic analysis

The thermoeconomic analysis is a methodology that computes the cost of each stream based on the costs of the systems, the exergy flow, the destroyed exergy, and the waste exergies. The thermoeconomic cost ($\dot{C}_{k,t}$) is calculated by a linear equation system solved by a matrix computation, which is composed of cost balance and auxiliary equations. The cost balance equation is given by:

$$\sum \dot{C}_{in,t} + \dot{Z}_{k,t} = \sum \dot{C}_{out,t} \tag{3}$$

where $\dot{Z}_{k,t}$ is a cost rate of the component, evaluated at the time step. Some auxiliary equations are required to complete the matrix and achieve a unique solution. These auxiliary equations relate the unit thermoeconomic cost ($c_{k,t}$) of different steams or with the unit cost of the fuel or the wastes, following the fuel-product principles [42]. The $c_{k,t}$ is obtained from the relation between the thermoeconomic cost and the exergy rate ($\dot{X}_{k,t}$) as [48]:

$$\dot{C}_{k,t} = c_{k,t}\dot{X}_{k,t} \tag{4}$$

The set of auxiliary equations implemented in this work follows the approach presented in [30]. However, the disaggregation level of the MED plant was simplified to only one device. Moreover, the present study includes a thermoeconomic analysis of the CSP and PV plant. Specifically, the hot and cold TES tanks present a dynamic behavior that consists of a volume and temperature variation of the molten salts [49]. Thus, a variation of the cost balance equation was proposed (Eq.5), including the term of cost accumulation rate ($\Delta\dot{C}_{CV,i,t}$) [44], which is related to the exergy accumulation term that is usually eliminated. The cost accumulation rate of the component can be separated as the cost stored at the beginning of the time step ($\dot{C}_{initial,i,t}$) and the cost stored at the final of the time step ($\dot{C}_{final,i,t}$).

$$\dot{C}_{in,k,t} - \dot{C}_{out,k,t} + \dot{Z}_{k,t} = \Delta\dot{C}_{CV,k,t} = (\dot{C}_{final,k,t} - \dot{C}_{initial,k,t}) \tag{5}$$

Both terms are related to the exergy stored by the molten salts (defined by the temperature in the tank) and the tanks volume at the time step. Thus, to complement the auxiliary equations, the following were proposed for each tank:

$$c_{final,k,t} = c_{out,k,t} \tag{6}$$

$$c_{initial,k,t} = c_{final,k,t-1} \tag{7}$$

The thermodynamic analysis was performed for every time step of the simulation (8760 h), in which the hot and cold TES tanks transfer the cost accumulated through each time step. Moreover, the streams considered as the products of the plant were the net electricity output and the freshwater chemical exergy flow [27,30]. Their unit costs were defined as Thermoeconomic Cost of Electricity (TCE) in $/MWh and the Thermoeconomic Cost of Water (TCW) in $/m^3. Finally, the daily, monthly and annual cost were computed from the results of the hourly cost rates by the following expression, where $Elec_{i,t}$ is the net electricity production in MWh, $Water_{i,t}$ is the water production in m^3 and T is the number of hours:

$$TCE = \frac{\sum_{t=1}^{T} \dot{C}_{el,t}}{\sum_{t=1}^{T} Elec_t} \tag{8}$$

$$TCW = \frac{\sum_{t=1}^{T} \dot{C}_{w,t}}{\sum_{t=1}^{T} Water_t} \tag{9}$$

4.3. Economic analysis

The economic analysis comprises the cost evaluation of the components to obtain the cost rates, which is obtained by the following expression in $/h:

$$\dot{Z}_{i,t} = \frac{A_f + f_{O\&M}}{O_{time,i}} Z_i \tag{10}$$

where $f_{O\&M}$ is the operation and maintenance factor that was set to 5%, $O_{time,i}$ is the annual operating time of the component in hours and the A_f is the amortization factor that depends on the interest rate and the plant's technical lifetime [30]. The total capital investment (Z_i) of the components or system considered were calculated, considering several cost correlations in the literature [9,45,50–56]. Likewise, the pipeline cost was updated with information reported in previous works adapted to particular conditions in Chile [9,21,57]. The Z functions are presented in detail in Appendix A.3 (Table A4). Finally, the annual operating time was computed from the performance of the plant, counting the number of hours that work at year each component.

5. Results and discussion

The study of the CSP + PV + MED plant was performed considering the meteorological conditions at Crucero located in northern Chile (Lat. − 22.24° S and Lon. − 69.51°), which presents a large number of days with high DNI levels throughout the year with a DNI total of 3389 kWh/m^2-yr [11]. Fig. 3 shows the yearly DNI profile, wherein February presents several cloudy days due to a local phenomenon in northern Chile known as the Altiplanic Winter. This phenomenon consists of moist air that comes from Bolivia that brings unsettled weather and occasional rain. This location is at 1000 m above

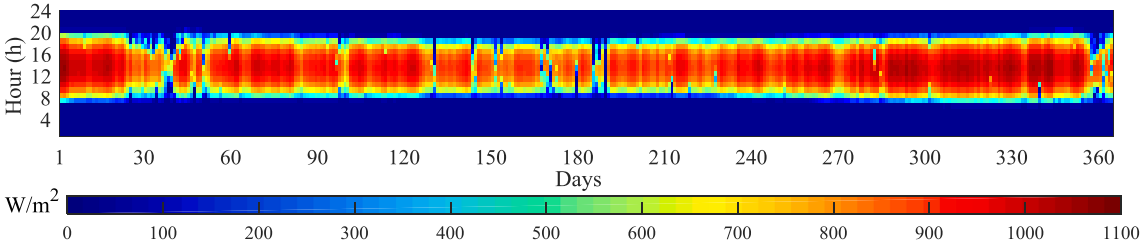

Fig. 3. DNI profile for the location at Crucero, Chile.

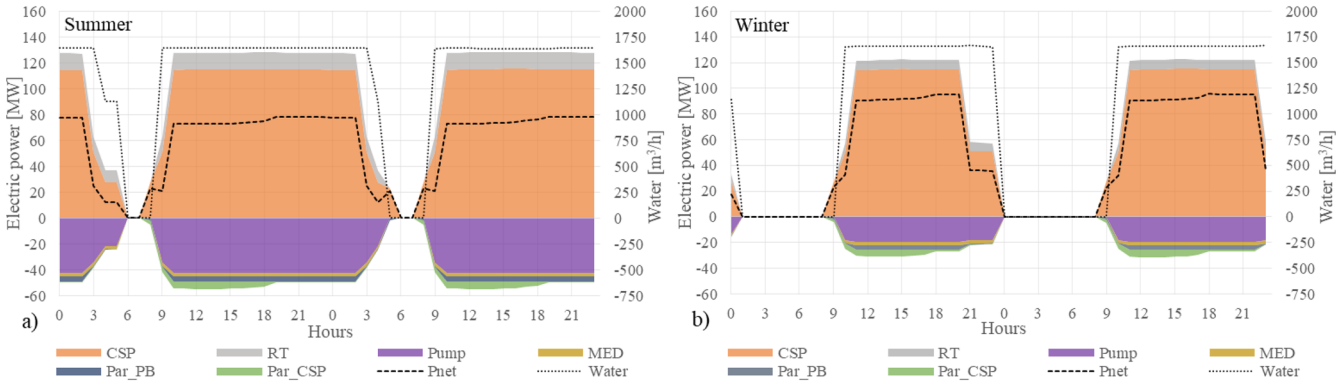

Fig. 4. Electric power balance and water production of the CSP + MED plant for three days in (a) summer (January 8-9th) and (b) winter (July 20-21th).

sea level and 100 km away from the coast, which was considered for the P/R system design and operation. The seawater temperature data was obtained for Antofagasta from [58], where the monthly profile was extracted, varying between 15.0 and 20.8 °C

In this section, the annual performance and thermoeconomic analysis of the CSP + PV + MED plant are presented, considering a configuration of 100 MW_e for the PV plant, a SM of 2.4, 12 h of TES, and four units for the MED plant. A comparison analysis was performed between the plant with and without the PV system, in order to understand the impact of the PV integration on the performance and the thermoeconomic indicators of the whole plant. A unidimensional sensitivity analysis is also presented, varying each one of the design parameters, showing the impact on the performance and the cost of the products. Finally, a multivariable parametric analysis is shown, where different optimum configurations that minimize both the thermoeconomic electric and water costs are analyzed.

5.1. Annual performance

Fig. 4 shows the hourly performance of the CSP + MED plant for two days in summer (from 8th to 9 ^{h} of January) and in winter (from 20th to 21th of July), in which the gross power production of the CSP plant (CSP) and the recovery turbine (RT) production, as well as, the power consumption of the seawater pumping system (Pump), the MED plant (MED), the parasitic of the power block (Par_PB) and the parasitic of the CSP (Par_CSP) are presented. It is observed that the CSP power is at full load during the day, and the water production (Water) is near to the nominal condition for summer and winter days, only varying the operating hours per day (approximately 22 h in summer and 15 h in winter). It is worth to mention that in summer, the power consumption of the seawater pumping system (Pump) reaches 43 MW_e, while during the winter it decreases to 21 MW_e, mainly because of the seawater temperature variation that reduces the inlet seawater mass flow rate. Thus, the power balance of the plant changes, obtaining a higher net output power (Pnet) during the winter months, but with lower operating hours.

In contrast, Fig. 5 shows the hourly performance of the CSP + MED system integrated with the PV plant, in which the gross power production of the PV plant (PV) and the dumped power in the PV plant (PV_dump) are also presented. In summer, it is observed that the power produced by the PV plant is around 80–95 MW, which forces the power block of the CSP plant to work at minimum part-load operation in order to complement the net output power to 100 MW_e. In this case, the MED plant works at part-load (around 60% thermal load), decreasing the power consumption of the seawater pumping system. Moreover, around noon, the PV plant reaches its maximum power output, and the electric power balance exceeds the nominal net output power, so part of the power from the PV plant is dumped. Also, the CSP parasitic consumption (Par_CSP) decreases because the TES system is charged, which forces to dump the energy excess from the CSP plant. At night, the power block and the MED plant operates at full load, with a net output power of 78 MW.

Conversely, in winter, the power production of the PV plant is about 70 MW, and the power block of the CSP plant complements to 100 MW_e, but the TES system is not completely charged during the daylight hours. Thus, the energy stored in the TES is not enough to operate during all-night, turning off the CSP and the MED plant between 4 and 6 am. Additionally, the MED plant is off during the daylight hours because the available steam is 60% of the nominal thermal load, and the plant needs 70% for the start-up process. Thus, the MED plant mainly works at between 10 and 12 h during the night. The main differences in the plant performance are that in summer the power block and the MED plant works 24 h, while in winter both systems are shut down, decreasing the daily water production.

Figs. 6 and 7 show the daily electric energy balance and the water production of the CSP + MED and CSP + PV + MED plants, respectively. In Fig. 6, it is observed significant variability in the total daily electric energy produced by the CSP plant and the net output electricity throughout the year (Pnet), which depends on the daily DNI. Likewise, the water production (Water) follows the power output of the CSP plant, evidencing that the MED plant operation depends on the power block operating hours. Moreover, it is shown a variation on the energy for seawater pumping (Pump) due to the changes in the seawater temperature and the daily operational hours of the MED plant.

For the case of the PV integration (Fig. 7), it is observed that the daily electric energy from the CSP plant is limited around 1500 MWh/day due to the combination with the PV plant. Moreover, the net output electricity remains stable during the year, having some variations for the cloudy days. Regarding the water production, it is detected two levels of daily water production, one at 35 dam^3/day and the other at 20 dam^3/day. The difference between the two levels is mainly due to the daily operational hours of the MED plant. During the days presenting high water production, the whole plant performed similarly to a summer day, in which the CSP plant and the MED plant worked 24 h. On the other hand, in the days with low water production, the plant performed similarly to a winter day in which the MED plant worked approximately 12 h during the night. These differences also affect the seawater pumping consumption and energy balances of the plant, leading to significant changes in the PV dumped energy.

Regarding the annual electricity balance and water production of the whole plant, Table 2 shows that the integration of the PV plant increases 30% of the total electric production and almost 48% of the net electricity production, compared to the CSP + MED plant. In addition to that, the CSP plant decreases its annual electric output due to the fact that it operates in a secondary role, increasing the solar energy dumped in the CSP solar field, and showing more part-load operation hours of the power block. The total parasitics consumption (Pump, MED, ACC, Par_PB and Par_CSP consumption) and the water production also

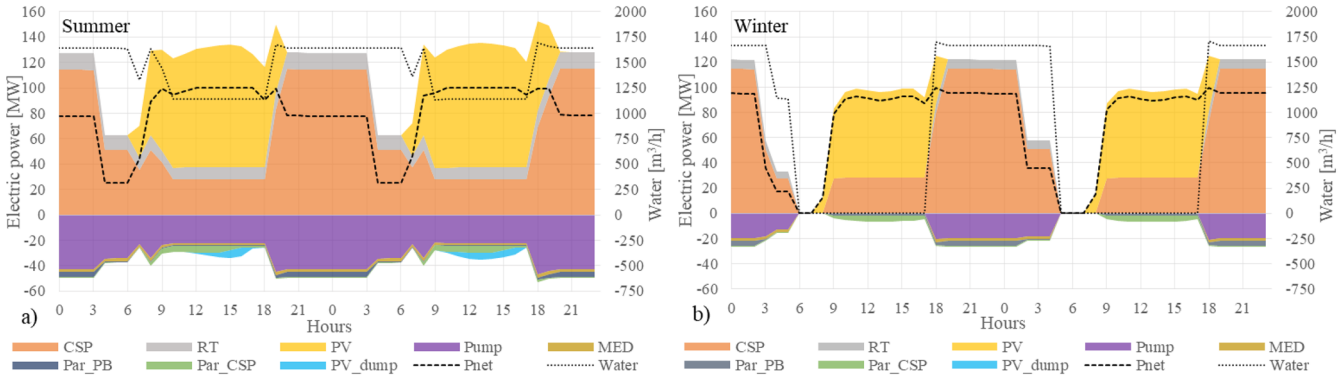

Fig. 5. Electric power balance and water production of the CSP + PV + MED plant for three days in (a) summer (January 8-9th) and (b) winter (July 20-21th).

decrease 10% and 17%, respectively, due to the fact that the CSP and MED plants reduce their annual hours of operation. In terms of the capacity factor (CF – ratio between the yearly power/water production and the maximum power/water production at nominal capacity), the CSP + MED plant achieves a power capacity factor of 51% and a water capacity factor of 68%, while the CSP + PV + MED plant obtained a power capacity factor of 76%, with a water capacity factor of 57%.

The PV plant integration allows storing more energy in the TES system during the daylight hours, increasing the net output electricity of the plant significantly and, in a first instance, the operational hours of the power block and the MED plant. However, these last two systems operate more hours at part-load under this configuration, causing an increase of the dumped energy of the CSP solar field and a decrease of the available CSP thermal energy in the annual balance, reducing the operational hours of the MED plant; and thus, the total water production. These results are in concordance with the results previously presented by Valenzuela et al. [24].

5.2. Thermoeconomic results

Daily TCE and TCW of the CSP + PV + MED plant are shown in Figs. 8 and 9, which illustrate the contribution of the five main systems of the plant (the PV plant, the CSP plant, the power block - PB, the MED plant, and P/R system). In Fig. 8, it is observed that the TCE presents an important contribution from the CSP plant and the P/R system, which are the two most expensive systems of the plant. Furthermore, the TCE shows a profile marked by two cost levels with some peaks that are related to cloudy days. The two cost levels are around 120 $/MWh and 160 $/MWh, and they are associated with the two levels of daily water production during the year. The main difference between these levels lies in the fact that the contribution of the P/R system increases significantly when the water production rises to 35 hm^3/day, meaning that the P/R system works for more hours and allocates more cost to the electricity produced. Besides that, it is observed that the cost contribution of the PV plant is small despite the amount of energy that is produced by this system, and the cost contribution of the MED plant to the TCE is almost negligible. Finally, the cost contribution of the CSP plant to the TCE presents small variations, mainly decreasing for the summer months and moderately increasing for winter days.

In contrast, Fig. 9 shows that the daily TCW presents a stable cost throughout the year, with some slight variations. The most significant change is attributable to the CSP contribution, which varies in the same form than observed for the TCE. Moreover, it is evidenced that the contribution of the MED plant and the P/R system are practically the same for each day. It is important to highlight that the TCW is not affected by the variation of the power consumption by the seawater pumping system during the year (see Fig. 7). Finally, the cost contribution of the PV plant and the power block to the TCW are small or negligible.

Fig. 10 show the monthly TCE and TCW obtained for the CSP + PV + MED plant, indicating that the TCE variation is mainly influenced by the CSP contribution, which moderately increases during the cloudy months (February, May, June, and July), and by the P/R system cost that is in terms of the water production. Meanwhile, the TCW presents only a small variation of the CSP cost contribution, also evidencing that it is not related to water production.

Table 3 shows the distribution of the total costs of the plant's main systems to the electricity and water costs in MM$ for the CSP + MED and CSP + PV + MED plants. In this way, the percentages represent the share of the total cost that is allocated to the electricity and water cost for each system. In addition that, it is evidenced that the cost contribution of the CSP plant and of the P/R system costs (which are the more expensive systems) are allocated to the electricity with 80% and 75% respectively for both cases. The distribution of the P/R system

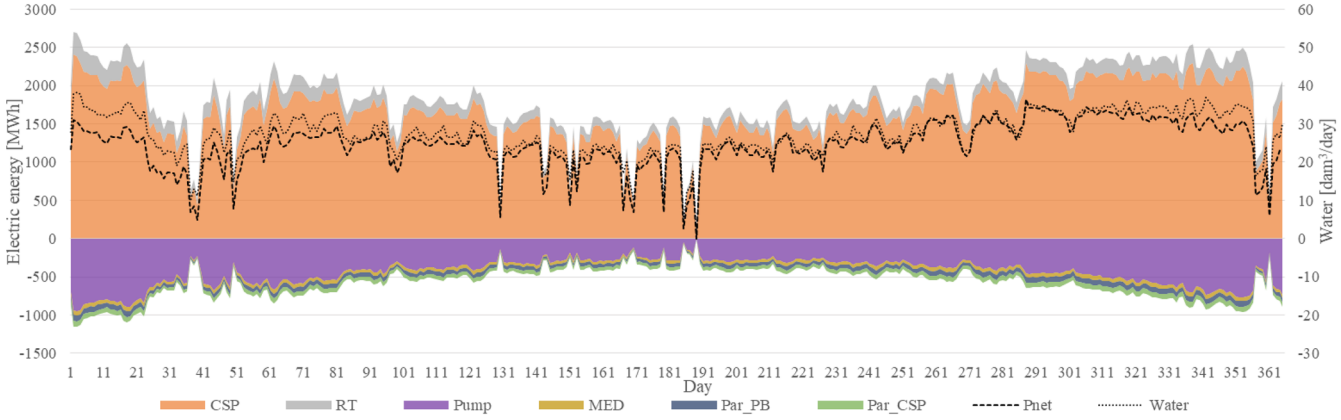

Fig. 6. Daily electric energy balance and water production of the CSP + MED plant.

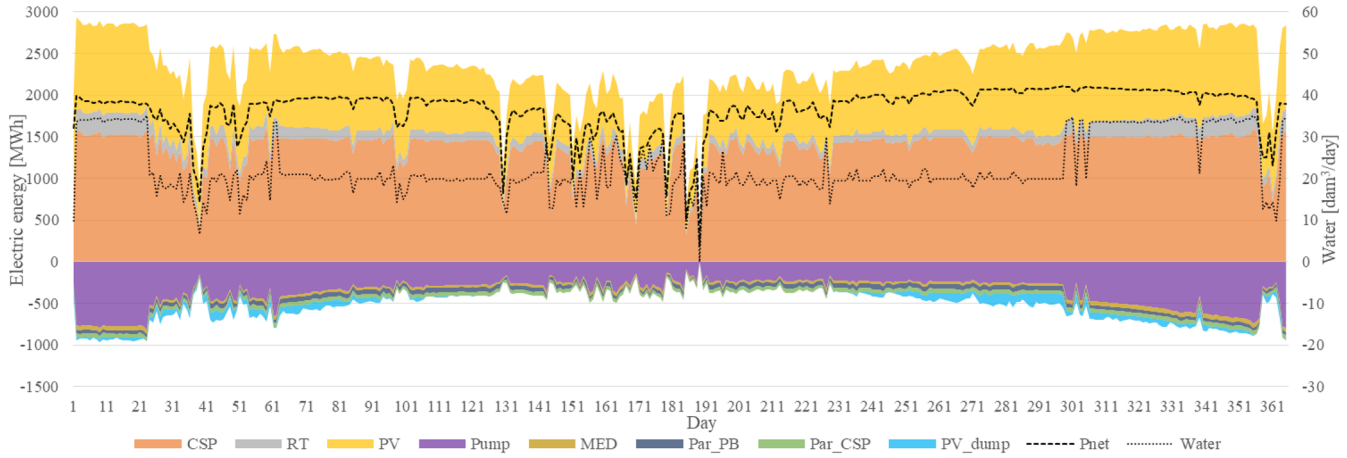

Fig. 7. Daily electric energy balance and water production of the CSP + PV + MED plant.

Table 2
CSP + PV + MED plant annual electricity distribution and water production.

Electricity production		CSP + MED		CSP + PV + MED	
CSP	[GWh]	605.6	91.4%	501.0	58.3%
PV	[GWh]	0.0	0.0%	310.5	36.1%
RT	[GWh]	57.1	8.6%	48.3	5.6%
Total	[GWh]	662.7	100.0%	859.8	100.0%
Electricity distribution					
Net	[GWh]	450.7	68.0%	668.3	77.7%
Pump	[GWh]	159.6	24.1%	131.9	15.3%
MED	[GWh]	15.0	2.3%	12.4	1.4%
Par_PB	[GWh]	18.8	2.8%	17.0	2.0%
Par_CSP	[GWh]	18.5	2.8%	16.1	1.9%
Dumped	[GWh]	0.0	0.0%	14.2	1.6%
Freshwater production					
Water production	[hm^3]	9.95		8.27	

occurred because approximately 25% of the seawater pumped to the plant location is transformed into freshwater, allocating this fraction of the cost to the water. The total cost of the power block is also mainly allocated to the electricity with more than 80% for both cases; similarly, the PV plant total cost is mainly allocated to the electricity (96%), while the MED total cost is almost wholly allocated to the water (99%). Hence, the operation and performance of the plant with the PV integration have a minor impact on the allocation of the electricity and water costs. Nevertheless, it worth to mention that the P/R system cost is composed of 95% of the cost of the two pipelines, which is associated with the length of the pipeline required. Therefore, the location of the plant with respect to the sea has a crucial role in the P/R system cost and the contribution of this system to the cost of the products, which can lead to lower costs if that distance is reduced.

The contribution of the cost of the main systems to the annual TCE and TCW for both plants is shown in Table 4. From the results, it is observed that the PV integration allows decreasing the TCE by 25%, while the TCW increases by 11%. Thus, the PV system integration main advantage is that the net output of electricity is increased, considering only a slight increase in the plant cost, which finally reduces the TCE dramatically. On the other hand, the CSP and MED plant operation are affected by the PV integration, which, in this case, reduces the water production. In contrast, the water maintains a similar cost allocation, so the TCW finally increases. Furthermore, the CSP + PV + MED plant could also improve the performance of the CSP and MED plant with smaller sizes of the PV plant, increasing the water production, which would result in a benefit on the TCW regarding the cost increase.

5.3. Sensitivity analysis

The operation and performance of the plant are affected by the configuration in terms of PV plant size, the CSP plant size (solar multiple and TES hours), and the number of MED units. According to the selected configuration, the operation and costs distribution would be different, which would change the annual TCE and TCW. Thus, a unidimensional analysis of the CSP + PV + MED plant has been firstly carried out, aiming to determine the impact of the selected configuration on the performance and costs. Secondly, a multivariable

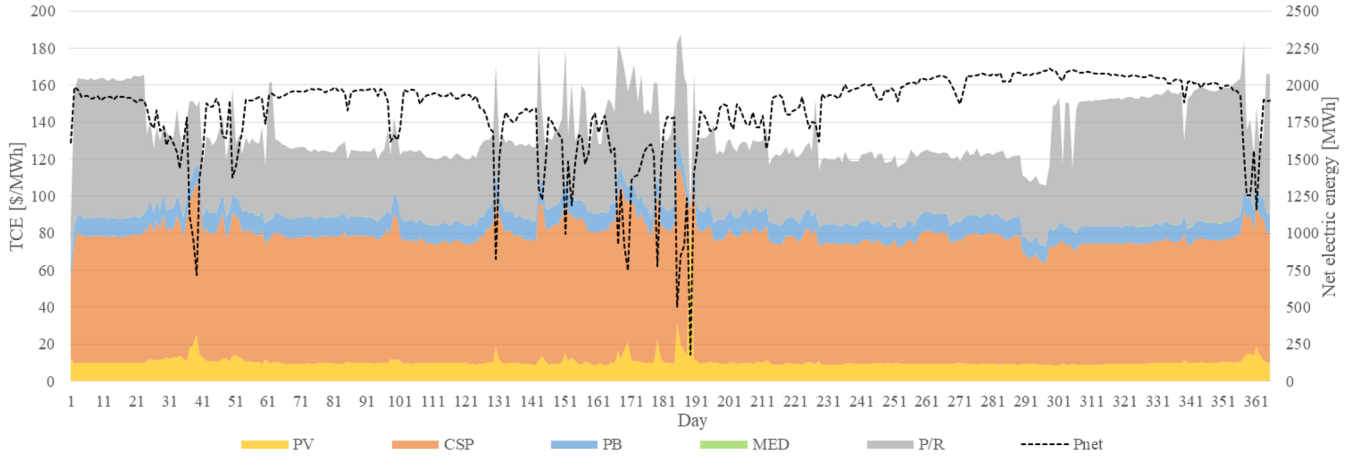

Fig. 8. Daily TCE considering the allocation of the PV, CSP, PB, MED, and P/R systems cost for a CSP + PV + MED plant configuration.

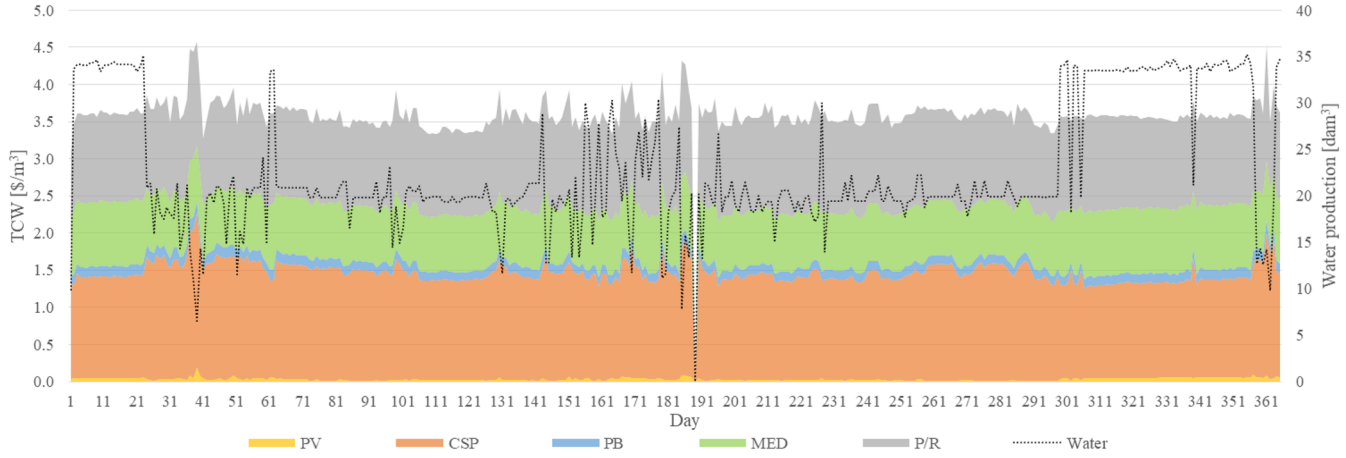

Fig. 9. Daily TCW considering the allocation of the PV, CSP, PB, MED, and P/R systems cost for a CSP + PV + MED plant configuration.

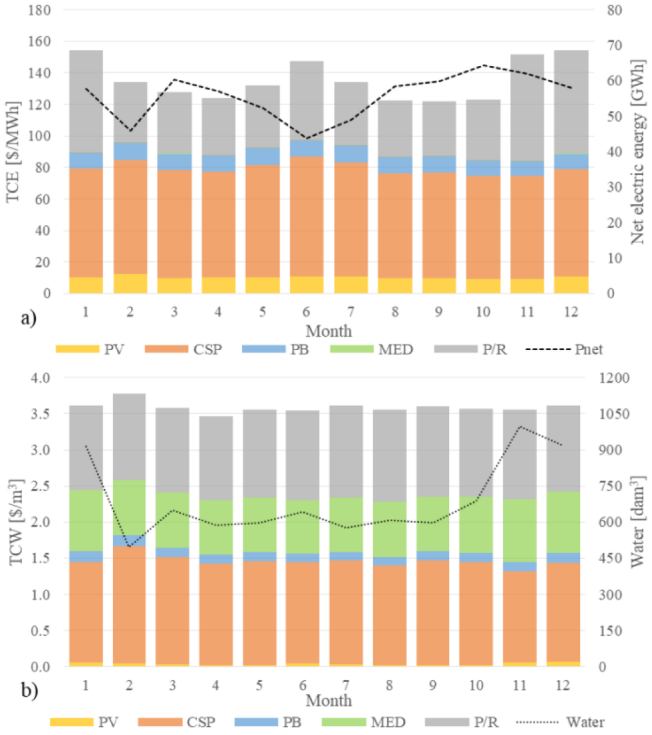

Fig. 10. Monthly (a) TCE and (b) TCW considering the allocation of the PV, CSP, PB, MED, and P/R systems costs of the CSP + PV + MED plant.

parametric study has been performed to find out which configurations would allow decreasing both the TCE and TCW.

5.3.1. CSP + PV + MED plant unidimensional analysis

The unidimensional analysis was carried out considering the base case exposed in section 5.1. Fig. 11 presents the annual energy balance of the plant and the water production, varying the PV size, the solar multiple (SM), the TES hours, and MED units.

In Fig. 11.a, it is observed that the net output electricity increases as the PV plant size is larger, showing that the PV dumped energy increases considerably from 125 MW onwards. In contrast, the electricity production by the CSP plant and the water production decreases from 75 MW up to 150 MW PV size, in which the power block and the MED plant operation hours are mainly limited to the night. Conversely, it is observed that the water production reaches a maximum for a PV size of 50 MW. For this size, the power block operates at more than 50% of the part-load, which allows the operation of the MED plant. Also, more energy is stored in the TES system during the day which enlarges the operation hours of the MED plant. In Fig. 11.b and 11.c, it is observed that the electricity production of the CSP plant is increased for larger SM and TES hours, which in turn leads to a rise in water production.

Fig. 11.d shows that the net electricity output remains stable with changes in the number of MED units. In contrast, water production presents an increase when the number of units varies from 1 to 3, and it remains in similar output as the number of units is increased above those values. This effect can be explained by the water capacity factor, which is represented in Fig. 12 for a different number of units, alongside the water production. As depicted in the figure, a capacity factor around 90% is achieved for a number of units between 1 and 3; however, above three units, it starts to decrease dramatically. For a lower

Table 3
Distribution of the PV, CSP, PB, MED, and P/R total costs to the electricity and the water costs in MM$ of the CSP + MED plant and CSP + PV + MED plant.

		Cost	PV	CSP	PB	MED	P/R	Total
CSP + MED	Total Cost	MM $	0	501.26	67.69	56.90	354.96	980.81
	Annualized cost	MM $	0	57.64	7.79	6.61	40.84	112.88
	Electricity	MM $	0	44.63	6.29	0.05	29.89	80.85
		%	0.0%	77.4%	80.7%	0.8%	73.2%	71.6%
	Water	MM $	0	13.02	1.50	6.56	10.95	32.03
		%	0.0%	22.6%	19.3%	99.2%	26.8%	28.4%
CSP + PV + MED	Total Cost	MM $	61.83	501.26	67.67	56.90	355.82	1043.48
	Annualized cost	MM $	7.11	57.60	7.79	6.61	40.94	120.05
	Electricity	MM $	6.82	45.92	6.72	0.05	30.87	90.37
		%	95.8%	79.7%	86.3%	0.8%	75.4%	75.3%
	Water	MM $	0.30	11.68	1.07	6.56	10.06	29.67
		%	4.2%	20.3%	13.7%	99.2%	24.6%	24.7%

Table 4
Contribution of the PV, CSP, PB, MED, and P/R systems costs to the annual TCE and TCW of the CSP + MED plant and CSP + PV + MED plant.

		Cost	PV	CSP	PB	MED	P/R	Total
CSP + MED	Electricity	$/MWh	0	99.00	13.94	0.12	66.31	179.38
		%	0.0%	55.2%	7.8%	0.1%	37.0%	100.0%
	Water	$/m^3	0	1.31	0.15	0.66	1.10	3.22
		%	0.0%	40.6%	4.7%	20.5%	34.2%	100.0%
CSP + PV + MED	Electricity	$/MWh	10.20	68.71	10.06	0.07	46.20	135.24
		%	7.5%	50.8%	7.4%	0.1%	34.2%	100.0%
	Water	$/m^3	0.04	1.41	0.13	0.79	1.22	3.59
		%	1.0%	39.4%	3.6%	22.1%	33.9%	100.0%

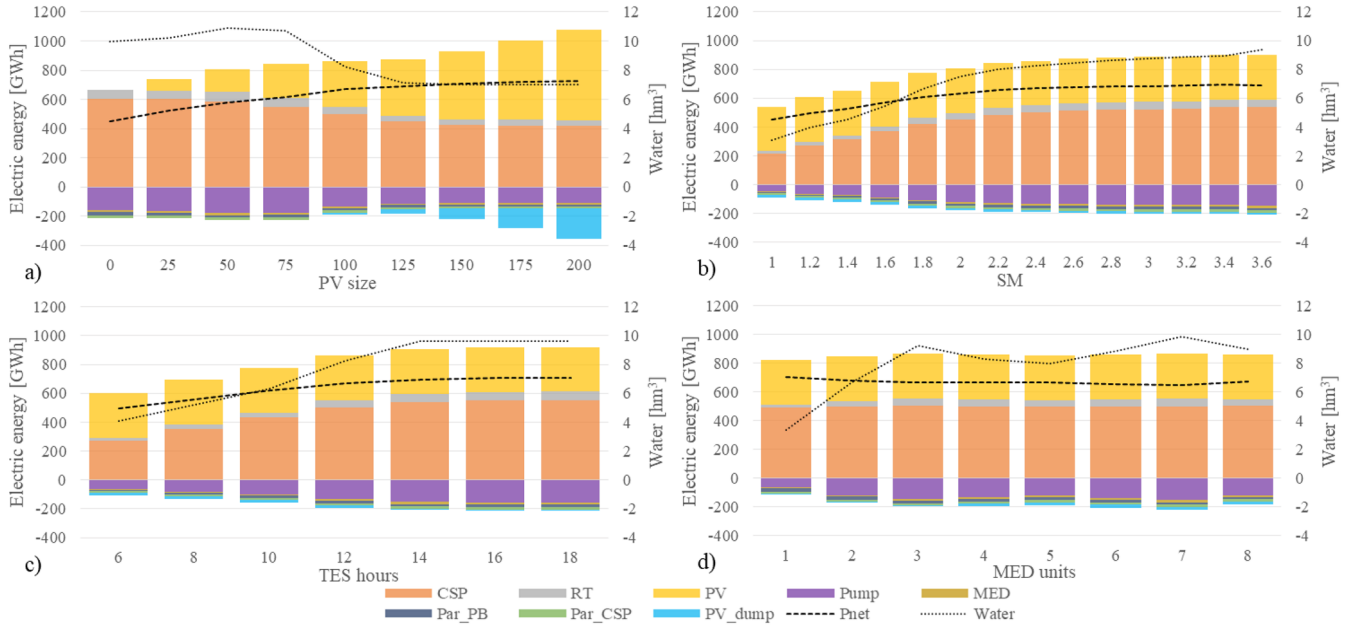

Fig. 11. Annual electric energy distribution and water production in a unidimensional parametric analysis varying: (a) PV size, (b) SM, (c) TES hours, and (d) MED units, considering a base case configuration with 100 MW of PV, 12 h of TES, a SM of 2.4 and 4 MED units.

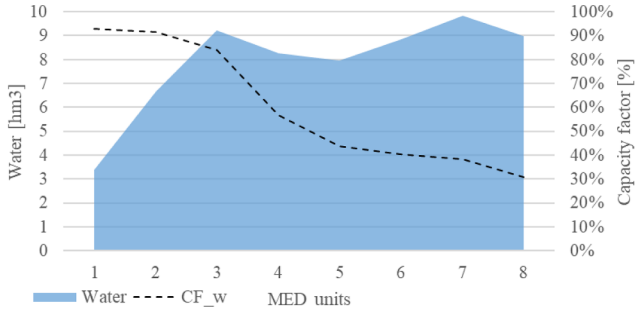

Fig. 12. Water production and water capacity factor for the different MED units.

number of units, the thermal energy required by the MED plant decreases, so the power block can provide enough thermal energy even at minimum part-load, increasing the operational hours of the MED plant. From four units onwards, the MED plant starts to operate more hours in winter mode, decreasing its capacity factor. For the maximum number of units, the MED plant works practically only at the night hours, and the capacity factor is the minimum one.

In terms of the cost results, Fig. 13 presents the contribution of the main systems to the TCE and TCW for the unidimensional analysis. In first instance, Fig. 13.a and Fig. 13.b show that the PV sizing has a relevant impact on the TCE and TCW. In Fig. 13.a it is observed that the TCE decreases, and the PV cost contribution increases for larger PV sizes, obtaining a minimum TCE at a PV size of 150 MW, where the PV dumped energy is compensated by the low costs of the PV plant. In contrast, in Fig. 13.b it is observed that TCW inversely varies to the water production, obtaining a minimum TCW at 50 MW PV size, in which the water production is maximized. This occurs because the PV sizing affects the CSP and MED operation hours despite the fact the PV cost contribution is negligible. Therefore, the PV sizing presents a contradictory role between the TCE and TCW.

In the case of the CSP plant size, it is observed that the TCE reaches a minimum for a SM of 2.2 and 14 h of TES (Fig. 13.c and Fig. 13.e), compensating the high CSP cost with the electricity production. In contrast, Fig. 13.d and Fig. 13.f show that the TCW tends to be lower as SM and TES hours are higher, and vice versa as SM and TES hours are lower and the water production decreases. In addition, the CSP cost contribution varies moderately for high SM and TES hours, evidencing the existence of a tradeoff between the increase of the CSP cost, the solar dumping in the solar field in summer months, and the increase of water production throughout the year. Following this, there is an optimum configuration of the CSP plant to achieve a minimum TCE. However, it is required an oversized CSP plant to increase the water production, achieving the minimum TCW.

Regarding the MED units, it is observed that the minimum TCE is found for 1 unit (Fig. 13.g), for which the contribution of the P/R system is the lowest. However, for a higher number of units, the contribution of the P/R system significantly increases, also causing a rise in the TCE. Conversely, it was found a minimum TCW for 3 MED units (Fig. 13.h), whereas the TCW gradually increases with a higher number

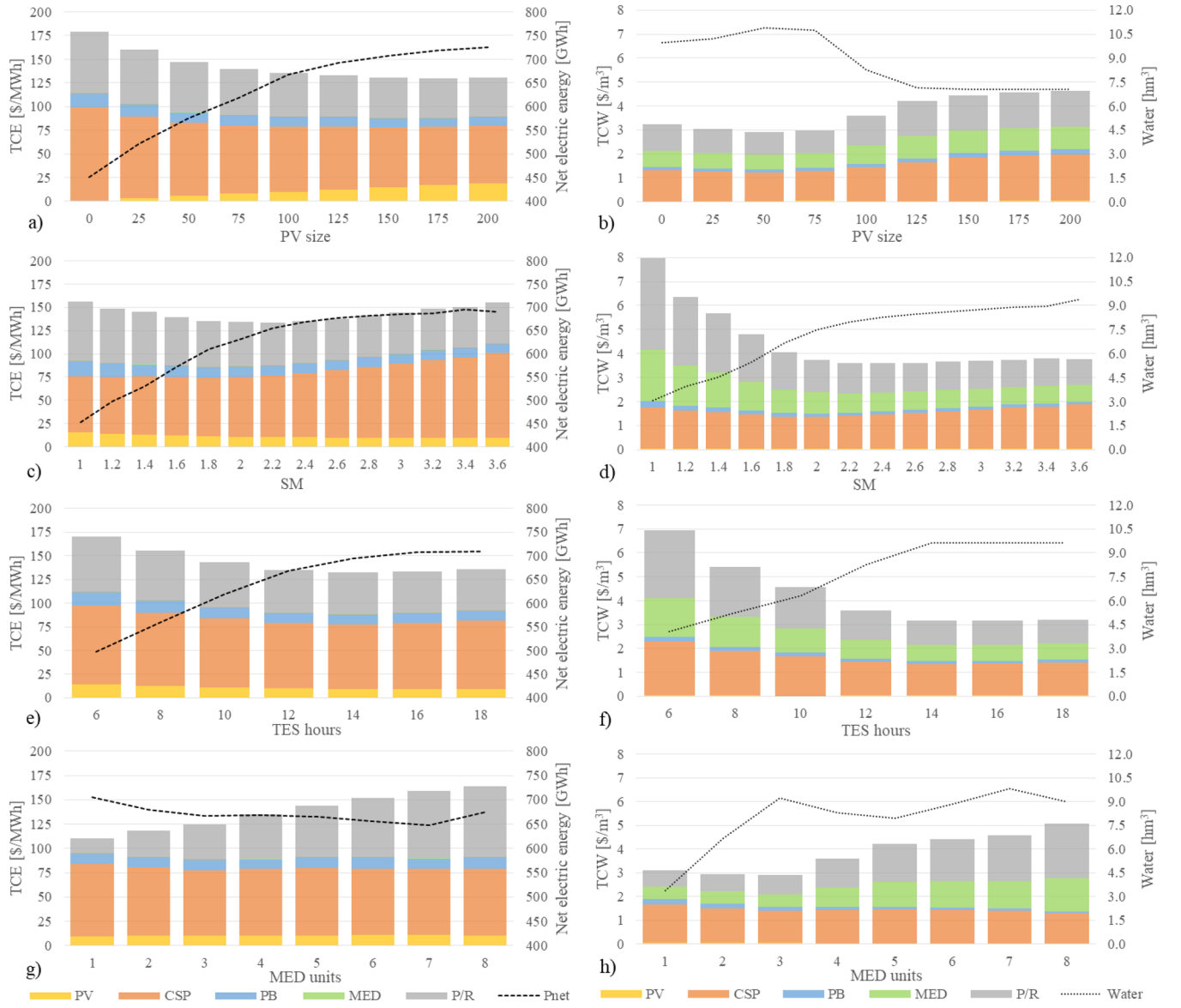

Fig. 13. Annual contribution of the PV, CSP, PB, MED and P/R systems costs in the TCE (a, c, e, g) and TCW (b, d, f, h) at the unidimensional parametric analysis varying: (a, b) PV size, (c, d) SM, (e, f) TES hours, and (g, h) MED units, considering a base case configuration of 100 MW of PV, 12 h of TES, 2.4 of SM and 4 MED units.

of units. Therefore, the lowest TCW would be found for a configuration that allows the MED plant to have a capacity factor over 85%. This configuration could be achieved with a combination of small PV plants and a large CSP solar field, but the number of MED units also has an essential role since it can change their performance according to the operation mode of the plant (summer or winter mode).

5.3.2. *Multivariable parametric analysis*

The parametric analysis was performed considering four configuration parameters of the plant (PV size, SM, TES hours, and MED units) within the range and the steps described in Table 5. The analysis considered 7056 configurations in total. Fig. 14 presents the results of TCE versus TCW clustered by the PV size and the MED units.

Table 5
Parametric multivariable parameters.

Parameters	Unit	Range	Step
PV size	[MW]	0–200	25
SM	[-]	1–3.6	0.2
TES hours	[h]	6–18	2
MED units	[-]	1–8	1

In Fig. 14.a, it is observed that the configurations with lower PV size (under 50 MW) achieve the lowest TCW; however, it presents TCE higher than 130 $/MWh, while with the PV size increasing, the scattered points are moved to lower TCE and higher TCWs. Moreover, it is observed a frontier where the lowest TCW (around 4 $/m^3) for a PV size above 125 MW is located. For these PV sizes, the power cycle is shut down during the day, limiting the operational hours of the MED plant. On the contrary, in Fig. 14.b, it is observed that the lowest TCEs are found for one MED unit. For higher MED units, the scattered points present higher TCEs with lower TCWs, showing that the cost of the P/R system is significant for the electricity cost.

Moreover, it is evident the existence of a Pareto frontier between the objective functions, the TCE and the TCW. Throughout this frontier, it is observed that the PV size gradually increases, while the MED units go from 1 for the lowest TCE to 5 for the lowest TCW. Furthermore, the configurations on the Pareto front are the results of a complex balance

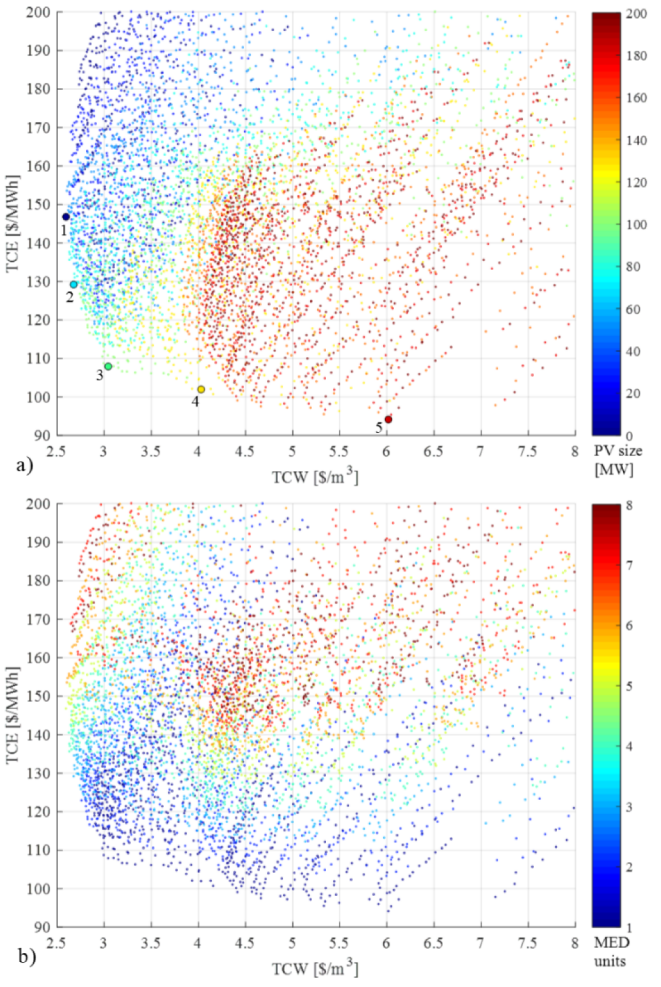

Fig. 14. TCW versus TCE of the CSP + PV + MED plant for different PV plant size (a) and the number of MED units (b). Circle marks represent five optimum configurations.

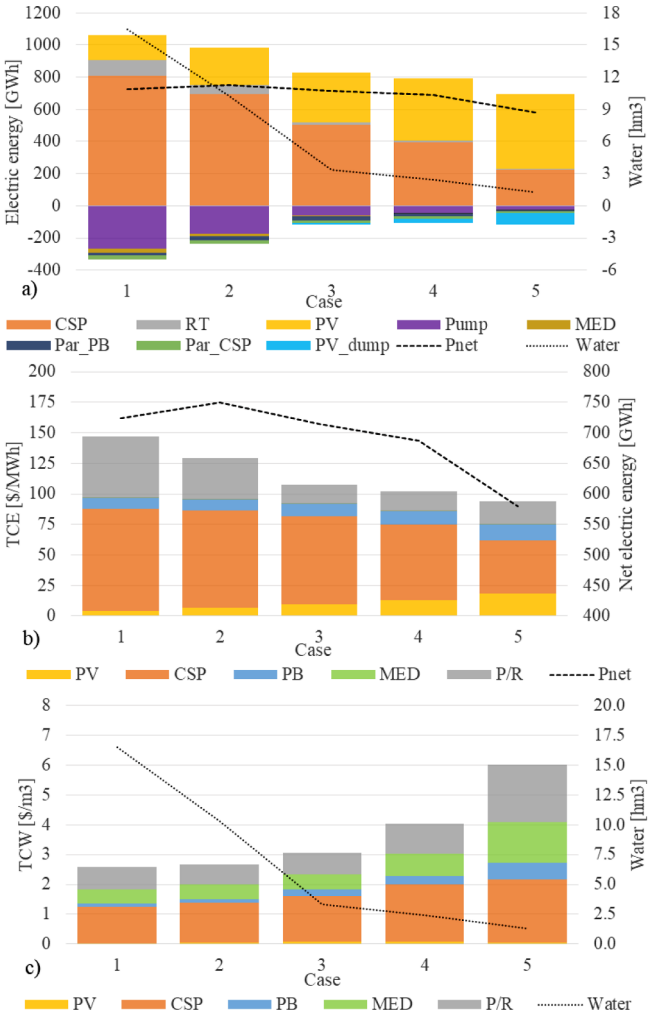

Fig. 15. (a) Annual energy balance and water production, (b) TCE, and (c) TCW with cost compositions for the 5 cases selected.

between the performance of the plant (electricity production, water production, PV dumped energy and solar field dumping) and the cost and thermoeconomic analysis (mainly the PV cost, CSP and P/R system cost). In Fig. 14.a, five points were selected along the frontier to analyze the different configurations considering both TCE and TCW. The detail of each case configuration is described in Table 6.

The results described in Table 6 indicate that the configuration that gives the minimum TCW (case 1) is a combination of a small PV plant with an oversized CSP plant and a large MED plant (5 units), while the configuration with the minimum TCE (case 5) is a combination of a large PV plant with an undersized CSP plant and only one MED unit. Cases 2, 3, and 4 are between the two formers configurations mentioned and show that the tendency of the PV plant size is just the opposite to the trend of the CSP + MED plant size.

Finally, Fig. 15 shows the energy balance, the water production, and the TCE and TCW for each case. It is observed a noticeable difference in the distribution of the electricity generation between the cases analyzed (Fig. 15.a). The case 1 presents a significant contribution from the CSP plant generation to the annual energy, also with a large parasitic consumption, while the case 5 has the main contribution of electric production from the PV plant, with a negligible parasitic consumption and a small amount of dumped energy. In terms of costs, it is observed that the TCE (Fig. 15.b) is influenced by the P/R system cost that has a higher contribution to the electricity cost if the water capacity factor and the number of the MED units are higher (case 1). Likewise, the TCW (Fig. 15.c) is mainly affected by the lower water capacity factors, which increases the cost rate of the MED and P/R system components (case 5), thus raising the water cost.

The results summarized in Table 6 also indicates that the power and water capacity factors tend to increase from case 5 to 3, while the

Table 6
Configuration and energy and thermoeconomic parameters of the five optimum configurations selected.

Case	PV [MW]	SM [-]	TES [h]	MED [units]	Electricity [GWh]	Water [hm^3]	CF_{el} [%]	CF_w [%]	C_{el} [MM $]	C_w [MM $]	TCE [$/MWh]	TCW [$/$m^3$]
1	50	3.4	16	5	723.88	16.48	82.63	90.31	106.18	42.84	146.68	2.60
2	75	3	16	3	749.74	10.29	85.59	93.99	96.78	27.58	129.08	2.68
3	100	2.2	14	1	714.33	3.36	81.54	92.12	77.00	10.25	107.80	3.05
4	125	1.8	12	1	686.98	2.40	78.42	65.82	69.97	9.69	101.85	4.03
5	150	1	8	1	578.99	1.29	66.09	35.26	54.45	7.75	94.04	6.02

number of MED units remains constant in 1 unit. However, from case 3 to 1, the capacity factors remain stable even though the MED units increase, which also raises the MED plant capacity; and therefore, the water production. Finally, it is evidenced that the PV plant integration allows to increase the production of electricity and to decrease the costs of the products, but depending on the PV plant size, it can benefit or hinder the operation of the CSP + MED system, and by consequence the water production. Furthermore, it was obtained a significant difference in the water production between all the cases, going from 1.3 to 16.5 hm^3, while the net electricity output varies between 579 and 724 GWh, which indicates that the demand requirements could play an important role in defining an adequate configuration.

6. Conclusions

The operation and performance of a CSP plant of 100 MW_e integrated with a PV and a MED plant have been assessed. A detailed thermoeconomic analysis has also been performed to analyze the distribution of the costs of the components in the products: electricity and water. The analysis was carried out considering an hourly simulation of the plant to take into account the irradiation and meteorological data variation and their effect on the operation of the plant. Main conclusions are presented as follows:

- The performance results indicate that PV integration to the CSP + MED plant mainly increases the net output electricity of the whole plant. Yet, as the secondary effect, it increases or decreases the water production depending on the PV and the CSP plant size. Moreover, two operation modes of the plant were identified for the PV integration: the summer mode, in which the CSP plant and MED plant work continuously 24 h with some of them at part-load, and the winter mode, where the CSP plant is turned off during the day, and the MED plant works fewer hours, reducing the daily water production.
- The thermoeconomic results show that the TCE is significantly reduced with the integration of the PV plant to the CSP + MED plant. However, the effect in the TCW is mostly related to water production, since the water presents almost the same cost allocation. Therefore, the impact of the PV integration on the TCW will finally depend on the operational hours of the MED plant.
- Regarding the results of the unidimensional analysis, it was obtained a minimum TCE for a large PV plant (150 MW), where the PV dumping is compensated by the low PV cost, and a minimum TCW for a small PV plant (50 MW), where the water production is maximized. Moreover, the minimum TCE was found for optimum configurations with medium or small CSP plants, while the minimum TCW was obtained for large CSP plant sizes with high SM and TES hours. Therefore, the PV and the CSP plant size present contradictory roles between the TCE and TCW. Furthermore, the numbers of MED units have an important role since it influences the plant operation and the P/R system cost. In this way, the minimum TCE is achieved with the minimum number of MED units, while the lower TCW can be reached with medium or high number of MED units with PV-CSP configurations that achieve a water capacity factors over 85%.
- The multivariable parametric analysis shows a Pareto frontier between the TCE and the TCW that evidences a solution space where both costs can be reduced. It was found that the best configuration in terms of minimum TCW is a combination of a small PV plant with an oversized CSP plant and a large MED plant (5 units), while the best configuration in terms of minimum TCE is a combination of a large PV plant with an undersized CSP plant and only one MED unit.
- The results have demonstrated the impact of the PV integration with a CSP + MED plant, using a methodology that allows assessing the actual allocation of the system costs into the products. These systems have a high complexity level; so, the methodology presented herein contributes to a proper assessment, considering several design parameters and independent variables related to the location. Beyond that, the analysis can be used as a design tool on a case-by-case basis.
- The plant location has shown to be a relevant factor due to the pumping consumption and the P/R system cost (second-highest system cost that is mainly composed of the two pipeline costs). However, locations closer to the coast may present lower radiations levels, which directly affects the PV and CSP production. These variables would change the thermoeconomic results and the configuration that would achieve the lowest TCE and TCW. However, the trade-off found in the Pareto frontier between the PV size, and CSP and MED size would be maintained. Therefore, further studies should analyze the impact of the altitude and distance from the coast versus the solar radiation of different locations in the thermoeconomic analysis of these systems.

CRediT authorship contribution statement

Carlos Mata-Torres: Conceptualization, Methodology, Software, Formal analysis, Writing - original draft, Visualization. **Patricia Palenzuela:** Methodology, Writing - review & editing. **Adriana Zurita:** Software, Writing - review & editing. **José M. Cardemil:** Supervision, Writing - review & editing. **Diego-César Alarcón-Padilla:** Supervision, Methodology. **Rodrigo A. Escobar:** Supervision, Conceptualization, Writing - review & editing, Resources.

Nomenclature

a_{ch}	Chemical exergy, kW
A_f	Amortization factor
CF	Capacity factor
$\dot{C}_k$	Thermoeconomic cost, $
c_k	Unit thermoeconomic cost, $/MWh
Dia	Diameter, m
Elec	Net electricity production, MWh
f	Factor
g	Gravity, m/s^2
h	Enthalpy, kJ/kg
ht	Height, m
L	Length, m
$\dot{m}$	Mass flow rate, kg/s
O_{time}	Annual operation time, h
P	Electric power, kW
Q	Heat, kW
s	Entropy, kJ/(kg K)
S	Negentropy, kW
T	Temperature, °C
TCE	Thermoeconomic cost of Electricity, $/MWh
TCW	Thermoeconomic cost of Water, $/$m^3$
UA	Heat exchanger thermal capacity, W/m^2
w	Salinity, kg_{salt}/kg_{water}
X_i	Exergy rate, kW
z	Altitude from the sea level, m
Z_i	Total Cost of Investment, $
$\dot{Z}_i$	Purchase cost rate, $/h

Greek Symbols

η	Efficiency
μ	Chemical potential, kJ/kg
ψ	Physical exergy kJ/kg

Subscripts and superscripts

boi	Boiler

br	Brine
cond	Condenser
csw	Cooling seawater
CV	Control Volume
cw	Cold side of the condenser
dea	Deaerator
dea_water	Deaerator water output
el	Electric
f	Feed
gen	Generator
hel	Heliostats
hot_PB	From the hot tank to the power block
in	Inlet
inHTF	Inlet Heat Transfer Fluid
k	k-th stream or component
MED	Multi-Effect Distillation
o	Reference condition
O&M	Operational and maintenance
out	Outlet
outHTF	Outlet heat transfer fluid
p_MED	Seawater pumping system power
PB_thermal	Power Block thermal
PV	Photovoltaic
rec	Receiver
rec_total	Receiver total
ref	Heliostats reflective total area
rh	Reheater
s	Steam
sg	Steam generator
st	Steam turbine
t	Time of the simulation
TES	Thermal Energy Storage
TES_cold	TES cold tank
TES_hot	TES hot tank
ttd	Terminal temperature difference
tur_MED	Recovery system turbine power
w	Water or freshwater
water	Freshwater

Acronyms

ACC	Air Cooled Condenser
CFWH	Closed Feed-Water Heater
CPH	Combined Power and Heat
CSP	Concentrating Solar Power
D	Desalination
DNI	Direct Normal Irradiation
EES	Engineering Equation solver
HTF	Heat Transfer Fluid
MED	Multi-Effect Distillation
P/R	Pumping and recovery
Par_CSP	Parasitic consumption from the CSP, MWh
Par_PB	Parasitic consumption from the Power Block
PB	Power Block
Pnet	Net output power
POA	Plane of the Array
PV	Photovoltaic
PV_dump	Dumped energy from the PV plant
RO	Reverse Osmosis
RT	Recovery Turbine
SGS	Steam Generation System
SM	Solar Multiple
TES	Thermal Energy Storage
TMY	Typical Meteorological year
TRNSYS	Transient System Simulation Program

Declaration of Competing Interest

The authors declare that they have no known competing financial interests or personal relationships that could have appeared to influence the work reported in this paper.

Acknowledgments

The authors appreciate the support from CONICYT/REDES 180174 “Solar-Assisted Desalination: perspectives and potential for Chile”, Fraunhofer Chile Research – Center of Solar Energy Technologies by the CORFO project 13CEI2-21803, and CONICYT/FONDAP 15110019 “Solar Energy Research Center“- SERC-Chile. Also, this research received funding from the Spanish government in the framework of the SOLTERMIN project (Ref. ENE2017-83973-R). Similarly, C. Mata-Torres would like to acknowledge the doctoral scholarship from CONICYT PFCHA/Doctorado Nacional 2018/21181537, and A. Zurita would like to acknowledge the doctoral scholarship from CONICYT PFCHA/Doctorado Nacional 2019/21191591.

Appendix A.1. Regression for the power block

The polynomial multi-variable regression of the power block was obtained considering a second-degree polynomial according to the structure of the Eq. (A.1) for each output (W_{net}, $\dot{m}_{cond}$, h_s and T_{outHTF}). The coefficients are presented in Table A1. The temperatures and mass flow rate inputs were in °C and kg/s. The units of the variables (W_{net}, $\dot{m}_{cond}$, h_s and T_{outHTF}) are obtained in kW, kg/s, kJ/kg and °C, respectively.

$$Variable = a_1 T_{amb} + a_2 T_{inHTF} + a_3 T_{inHTF} T_{amb} + a_4 \dot{m}_{inHTF} + a_5 \dot{m}_{inHTF} T_{amb} + a_6 \dot{m}_{inHTF} T_{inHTF} + a_7 + a_8 \dot{m}_{inHTF}{}^2 + a_9 T_{inHTF}{}^2 + a_{10} T_{amb}{}^2 \quad (A.1)$$

Table A1
Coefficients of the Power Block regressions.

Variables	W_{net}	$\dot{m}_{cond}$	h_s	T_{outHTF}
Coefficients	*a*	*b*	*c*	*d*
1	802.260449	−0.10035345	7.89993818	−0.00254884
2	252.93949	−0.09569104	6.76346253	−0.52047855
3	−1.43221726	9.79E-05	0.00503829	2.29E-06
4	−377.049784	−0.20563778	−0.7892647	−0.10499621
5	−0.51398804	4.61E-05	−0.00022502	−1.74E-06
6	1.0358509	0.00057948	−0.00106855	0.00033949
7	−107328.177	25.1184066	734.935064	459.72985
8	0.00685085	−5.97E-06	0.00086653	−3.70E-05
9	−0.13462605	9.03E-05	−0.00644664	0.00027109
10	−0.43974145	0.00047372	−0.0184497	2.49E-05

Appendix A.2. Regression for the MED plant

The polynomial multi-variable regression of the MED plant was calculated considering a second-degree polynomial according to the structure of the Eq. (A.2) and the design parameters mentioned in Section 2.3. The variables calculated were: the freshwater mass flow rate ($\dot{m}_{water}$), the feed seawater mass flow rate ($\dot{m}_f$), the steam temperature at the inlet of the first effect (T_s), the freshwater outlet temperature (T_{water}), the brine outlet temperature (T_{br}), and the seawater temperature at the outlet of the last condenser (T_{csw}). The coefficients are presented in Table A2. In the equation, $\dot{m}_s$ is the thermal load (between 0.4 and 1), which represent the inlet steam mass flow rate flow fraction with respect to the design mass flow rate (11.45 kg/s), h_{steam} is steam enthalpy in kJ/kg, and T_{sw} is the seawater temperature in ˚C. The variables are obtained in kg/s for the mass flow rates and ˚C for the temperatures.

$$Variable = a_1 T_{sw} + a_2 h_{steam} + a_3 h_{steam} T_{sw} + a_4 \dot{m}_s + a_5 \dot{m}_s T_{sw} + a_6 \dot{m}_s h_{steam} + a_7 + a_8 \dot{m}_s{}^2 + a_9 h_{steam}{}^2 + a_{10} T_{sw}{}^2 \quad (A.2)$$

For the regression of the cooling seawater mass flow rate ($\dot{m}_{csw}$), it was considered a third-degree polynomial with four inputs: $\dot{m}_s$, h_{steam}, T_s and T_{sw}, to achieve and NRMSD under 1%. The T_s is taken from the previous regression result. Table A3 presents the exponents associated to each input and the regression coefficients.

Table A2
Coefficients of the MED plant regressions.

Variable	$\dot{m}_{water}$	$\dot{m}_f$	T_s	T_{water}	T_{br}	T_{csw}
Coefficients	a	b	c	d	e	f
1	0.63908436	1.43791024	0.1118902	0.0152036	−2.51E−14	0.67584346
2	0.03026028	0.06808431	0.00827368	0.00029074	−7.19E−16	0.00365412
3	−0.0001026	−0.00023084	−1.75E−05	−2.28E−06	3.95E−18	−9.21E−05
4	100.126441	225.284257	28.7551129	1.08804772	−3.34E−13	14.6611841
5	−0.37237943	−0.8378414	−0.06510767	−0.00842487	3.87E−15	−0.35051739
6	0.02093228	0.0470977	0.00288226	4.02E−05	8.27E−17	−0.00390137
7	−61.079828	−137.427406	28.236119	34.3531461	34.8487	21.9652553
8	−35.8524985	−80.6682349	−10.3487037	−0.35109641	2.19E−14	−2.52450911
9	−2.95E−06	−6.64E−06	−8.07E−07	−2.29E−08	1.09E−19	−1.79E−07
10	−0.00610317	−0.0137323	−0.00113787	−0.0001722	2.74E−16	−0.0098178

Table A3
Input exponent and coefficients of the cooling seawater mass flow rate regression.

Coefficients	a	$\dot{m}_s$	h_{steam}	T_s	T_{sw}
1	−242.968952	0	0	0	1
2	42.2092227	0	0	0	2
3	5984.59346	0	0	1	0
4	−17.9638018	0	0	1	1
5	−1.67856066	0	0	1	2
6	−279.742341	0	0	2	0
7	0.42978931	0	0	2	1
8	−34.1529419	0	1	0	0
9	0.65231287	0	1	0	1
10	0.00944732	0	1	0	2
11	2.15213348	0	1	1	0
12	−0.00873418	0	1	1	1
13	−0.0314104	0	1	2	0
14	−0.00078664	0	2	0	0
15	−8.25E−05	0	2	0	1
16	−3.85E−05	0	2	1	0
17	0	1	0	0	0
18	3258.27084	1	0	0	1
19	37.2179266	1	0	0	2
20	−316.661128	1	0	1	0
21	−85.9012176	1	0	1	1
22	9.22684737	1	0	2	0
23	113.402404	1	1	0	0
24	0.85206171	1	1	0	1
25	−3.4561388	1	1	1	0
26	0.02422076	1	2	0	0
27	0	2	0	0	0
28	629.42245	2	0	0	1
29	−559.977085	2	0	1	0
30	40.3279563	2	1	0	0
31	0	0	0	0	0
32	0	3	0	0	0
33	4.97E−07	0	3	0	0
34	3.33608596	0	0	3	0
35	0.25119342	0	0	0	3

Appendix A.3. Cost function of the plant

Table A4
Cost function correlation for each plant component.

Component	Total cost of investment equations	Ref.
Heliostats	$Z_{hel} = 160\$/m^2 A_{ref}$ (A.3)	[22,53] *1
Receiver and Tower	$Z_{tower} = 95,000\$/m(ht_{tower} - ht_{rec})$ (A.4) $Z_{rec} = 140\$/kW_t Q_{receiver}$ (A.5) $Z_{rec\_total} = Z_{rec} + Z_{tower}$ (A.6)	Assumption[54] *1
TES system	$Z_{TES} = 29\$/kWh_t TES_{hours} Q_{PB\_thermal}$ (A.7) $Z_{TES\_hot} = 0.6 Z_{TES}$ (A.8) $Z_{TES\_cold} = 0.4 Z_{TES}$ (A.9)	[55] *1
PV plant	$Z_{PV} = 0.45\$/W_e P_{PV}$ (A.10)	[56]
Inverter	$Z_{inverter} = 0.25\$/W_e P_{PV}$ (A.11)	[56]
Steam generator	$Z_{boi} = 208582 \frac{\$}{kgs} \dot{m}_{sg}^{0.8} e^{\left(\frac{P_e - 28}{150}\right)} F_{AN} F_{AT} F_{SHRH}$ (A.12) $F_{AN} = 1 + \left(\frac{1 - 0.95}{1 - \eta_1}\right)^7$ (A.13) $F_{AT} = 1 + 5e^{\left(\frac{T_1 - 593}{10.42}\right)}$ (A.14) $F_{SHRH} = 1 + \frac{Tsg_{out} - Tsg_{in}}{Tsg_{out}} + \left(\frac{\dot{m}_{sg}}{\dot{m}_{rh}}\right)\frac{(Trh_{out} - Trh_{in})}{Trh_{out}}$ (A.15) $Z_{sg} = (1 - f_{rh}) Z_{boi}$ (A.16) $f_{rh} = 0.12$ (A.17)	[50–52]
Re-heater	$Z_{rh} = f_{rh} Z_{boi}$ (A.18)	[51]
Turbine	$Z_{st} = 3880.5 \frac{\$}{kW^{-0.7}} P_{st}^{0.7} \left[1 + \left(\frac{0.05}{1 - \eta_{st}}\right)^3\right]\left[1 + 5e^{\left(\frac{T_a - 886}{10.42}\right)}\right]$ (A.19)	[50,52]
PB Pump	$Z_{pump} = 705.48 \frac{\$}{kgs} P_{pump}^{0.71}\left(1 + \frac{0.2}{1 - \eta_{pump}}\right)$ (A.20)	[50,52]
Condenser	$Z_{cond} = \left(\frac{1}{T_o e_1}\right)\left\{217\left[0.247 + \left(\frac{1}{3.24 V_{cw}^{0.8}}\right)\right]\ln\left(\frac{1}{1 - e_1}\right) + 138\right\}\left(\frac{1}{1 - \eta_{cond}}\right) S$ (A.21) $e_1 = \frac{Tcw\_out - Tcw\_in}{Tin - Tcw\_out}$; $\eta_c = \frac{T_o(s_{in} - s_{out})}{h_{in} - h_{out}}$ (A.22)	[51]
Deaerator	$Z_{dea} = 145315 \frac{\$}{kW^{-0.7}} \dot{m}_{dea\_water}^{0.7}$ (A.23)	[50,52]
CFWH	$Z_{CFWH,i} = 66 Q_{CFWH}\left(\frac{1}{T_{TTD,i} + a}\right)^{0.1} (10\Delta P_t)^{-0.08}(10\Delta P_s)^{-0.04}$ (A.24) $a = 6$ for high pressure FWH and $a = 4$ for low pressure FWH	[50]
Generator	$Z_{gen} = 60 P_{gen}^{0.95}$ (A.25)	[50,51]
MED plant	$Z_{MED} = 350 A_{MED}^{0.95}$ (A.26)	[30,45]
P/R system(seawater pump, recovery turbine and pipeline)	$Z_{pipe} = 2^{0.9} C_{pipe}(1000 L_{pipe})$ (A.27) $C_{pipe} = 1200 Dia_{pipe}^{1.8333}$ (A.28) $Z_{pump} = 4940 P_{pump}^{0.7231}$ (A.29) $Z_{rec\_tur} = 7410 P_{rec\_tur}^{0.7231}$ (A.30) $Z_{P/R\_pump} = Z_{pump} + \frac{Z_{pipe}}{2}$ (A.31) $Z_{P/R\_recovery} = Z_{tur\_rec} + \frac{Z_{pipe}}{2}$ (A.32)	Assumption[9,21,57]

*1 The CSP cost data base implemented is in concordance with the values reported by the CSP Association of Chile in 2019, which represent costs reported in the literature for central-receiver plants [53–55,59–61] validated by the industry in Chile.

References

[1] Ahmed FE, Hashaikeh R, Hilal N. Solar powered desalination – Technology, energy and future outlook. Desalination 2019;453:54–76. https://doi.org/10.1016/j.desal.2018.12.002.

[2] Shenvi SS, Isloor AM, Ismail AF. A review on RO membrane technology: Developments and challenges. Desalination 2015;368:10–26. https://doi.org/10.1016/j.desal.2014.12.042.

[3] Mayor B. Growth patterns in mature desalination technologies and analogies with the energy field. Desalination 2019;457:75–84. https://doi.org/10.1016/j.desal.2019.01.029.

[4] Shahzad MW, Burhan M, Ang L, Choon Ng K. Energy-water-environment nexus underpinning future desalination sustainability. Desalination 2017;413:52–64. https://doi.org/10.1016/j.desal.2017.03.009.

[5] Al-Karaghouli A, Kazmerski LL. Energy consumption and water production cost of conventional and renewable-energy-powered desalination processes. Renew Sustain Energy Rev 2013;24:343–56. https://doi.org/10.1016/j.rser.2012.12.064.

[6] Sola I, Sánchez-Lizaso JL, Muñoz PT, García-Bartolomei E, Sáez CA, Zarzo D. Assessment of the requirements within the environmental monitoring plans used to evaluate the environmental impacts of desalination plants in Chile. Water 2019;11:1–17. https://doi.org/10.3390/w11102085.

[7] Comision Chilena del Cobre. Consumo de agua en la minería del cobre al 2018. 2019.

[8] Comision Chilena del Cobre. Forecast for water consumption in the copper mining industry, 2018-2029. 2018.

[9] Herrera-León S, Lucay FA, Cisternas LA, Kraslawski A. Applying a multi-objective optimization approach in designing water supply systems for mining industries. The case of Chile. J Clean Prod 2019;210:994–1004. https://doi.org/10.1016/j.jclepro.2018.11.081.

[10] Concha F, Castro S, Vergara M. Economic Evaluation of Alternatives for Using Desalinated and Non-Desalinated Seawater in Cu/Mo Flotation Plants. 5thInternational Congr Water Manag Min 2016:1–12.

[11] Escobar RA, Cortés C, Pino A, Salgado M, Pereira EB, Martins FR, et al. Estimating

the potential for solar energy utilization in Chile by satellite-derived data and ground station measurements. Sol Energy 2015;121:139–51. https://doi.org/10.1016/j.solener.2015.08.034.
[12] Zurita A, Castillejo-Cuberos A, García M, Mata-Torres C, Simsek Y, García R, et al. State of the art and future prospects for solar PV development in Chile. Renew Sustain Energy Rev 2018;92:701–27. https://doi.org/10.1016/j.rser.2018.04.096.
[13] Alhaj M, Al-Ghamdi SG. Why is powering thermal desalination with concentrated solar power expensive? assessing economic feasibility and market commercialization barriers. Sol Energy 2019;189:480–90. https://doi.org/10.1016/j.solener.2019.07.046.
[14] Mohammadi K, Saghafifar M, Ellingwood K, Powell K. Hybrid concentrated solar power (CSP)-desalination systems: a review. Desalination 2019;468:114083https://doi.org/10.1016/j.desal.2019.114083.
[15] Palenzuela P, Zaragoza G, Alarcón-Padilla DC. Characterisation of the coupling of multi-effect distillation plants to concentrating solar power plants. Energy 2015;82:986–95. https://doi.org/10.1016/j.energy.2015.01.109.
[16] Palenzuela P, Alarcón-Padilla DC, Zaragoza G. Large-scale solar desalination by combination with CSP: Techno-economic analysis of different options for the Mediterranean Sea and the Arabian Gulf. Desalination 2015;366:130–8. https://doi.org/10.1016/j.desal.2014.12.037.
[17] Moser M, Trieb F, Fichter T. Potential of Concentrating Solar Power Plants for the Combined Production of Water and Electricity in MENA Countries. J Sustain Dev Energy, Water Environ Syst 2013;1:122–41. https://doi.org/10.13044/j.sdewes.2013.01.0009.
[18] Ortega-Delgado B, Garcia-Rodriguez L, Alarcón-Padilla D-C. Thermoeconomic comparison of integrating seawater desalination processes in a concentrating solar power plant of 5 MWe. Desalination 2016;392:102–17. https://doi.org/10.1016/j.desal.2016.03.016.
[19] Sharan P, Neises T, Mctigue JD, Turchi C. Cogeneration using multi-effect distillation and a solar-powered supercritical carbon dioxide Brayton cycle. Desalination 2019;459:20–33. https://doi.org/10.1016/j.desal.2019.02.007.
[20] Mata-Torres C, Escobar RA, Cardemil JM, Simsek Y, Matute JA. Solar polygeneration for electricity production and desalination: Case studies in Venezuela and northern Chile. Renew Energy 2017;101:387–98. https://doi.org/10.1016/j.renene.2016.08.068.
[21] Hoffmann JE, Dall EP. Integrating desalination with concentrating solar thermal power: a Namibian case study. Renew Energy 2018;115:423–32. https://doi.org/10.1016/j.renene.2017.08.060.
[22] Zurita A, Mata-Torres C, Valenzuela C, Felbol C, Cardemil JM, Guzmán AM, et al. Techno-economic evaluation of a hybrid CSP + PV plant integrated with thermal energy storage and a large-scale battery energy storage system for base generation. Sol Energy 2018;173:1262–77. https://doi.org/10.1016/j.solener.2018.08.061.
[23] Starke AR, Cardemil JM, Escobar RA, Colle S. Multi-objective optimization of hybrid CSP+PV system using genetic algorithm. Energy 2018;147:490–503. https://doi.org/10.1016/j.energy.2017.12.116.
[24] Valenzuela C, Mata-Torres C, Cardemil JM, Escobar RA. CSP + PV hybrid solar plants for power and water cogeneration in northern Chile. Sol Energy 2017;157:713–26. https://doi.org/10.1016/j.solener.2017.08.081.
[25] Leiva-Illanes R, Escobar R, Cardemil JM, Alarcón-Padilla D-C. Comparison of the levelized cost and thermoeconomic methodologies – Cost allocation in a solar polygeneration plant to produce power, desalted water, cooling and process heat. Energy Convers Manag 2018;168:215–29. https://doi.org/10.1016/j.enconman.2018.04.107.
[26] Kouta A, Al-Sulaiman F, Atif M, Bin Marshad S. Entropy, exergy, and cost analyses of solar driven cogeneration systems using supercritical CO2 Brayton cycles and MEE-TVC desalination system. Energy Convers Manag 2016;115:253–64. https://doi.org/10.1016/j.enconman.2016.02.021.
[27] Catrini P, Cipollina A, Micale G, Piacentino A, Tamburini A. Exergy analysis and thermoeconomic cost accounting of a Combined Heat and Power steam cycle integrated with a Multi Effect Distillation-Thermal Vapour Compression desalination plant. Energy Convers Manag 2017;149:950–65. https://doi.org/10.1016/j.enconman.2017.04.032.
[28] Wellmann J, Meyer-Kahlen B, Morosuk T. Exergoeconomic evaluation of a CSP plant in combination with a desalination unit. Renew Energy 2017;128:586–602. https://doi.org/10.1016/j.renene.2017.11.070.
[29] Leiva-Illanes R, Escobar R, Cardemil JM, Alarcón-Padilla D-C. Thermoeconomic assessment of a solar polygeneration plant for electricity, water, cooling and heating in high direct normal irradiation conditions. Energy Convers Manag 2017;151:538–52. https://doi.org/10.1016/j.enconman.2017.09.002.
[30] Mata-Torres C, Zurita A, Cardemil JM, Escobar RA. Exergy cost and thermoeconomic analysis of a Rankine Cycle + Multi-Effect Distillation plant considering time-varying conditions. Energy Convers Manag 2019;192:114–32. https://doi.org/10.1016/j.enconman.2019.04.023.
[31] Mata-Torres C, Zurita A, Cardemil JM, Escobar RA. Thermoeconomic Analysis of a CSP+PV+MED Plant in Chile: Assessing the Impact of the PV Plant Integration. Proc. 32nd Int. Conf. Effic. Cost, Optim. Simul. Environ. Impact Energy Syst. ECOS 2019, Wroclaw: 2019.
[32] Starke AR, Cardemil JM, Escobar RA, Colle S. Assessing the performance of hybrid CSP + PV plants in northern Chile. Sol Energy 2016;138:88–97. https://doi.org/10.1016/j.solener.2016.09.006.
[33] Turchi CS, Heath GA. Molten Salt Power Tower Cost Model for the System Advisor Model (SAM). 2013. doi:10.2172/1067902.
[34] Blair N, Dobos AP, Freeman J, Neises T, Wagner M, Ferguson T, et al. System Advisor Model, SAM 2014.1.14: General Description. 2014.
[35] Schwarzbözl P, Eiden U, Pitz-Paal R, Zentrum D, Scott J. A TRNSYS Model Library for Solar Thermal Electric Components (STEC) Reference Manual. 2006.
[36] National Renewable Energy Laboratory. System Advisor Model (SAM) 2018.
[37] Patnode AM. Simulation and performance evaluation of parabolic trough solar power plants. 2006.
[38] Ortega-Delgado B, Palenzuela P, Alarcón Padilla D-C. Parametric study of a multi-effect distillation plant with thermal vapor compression for its integration into a Rankine cycle power block. Desalination 2016;394:18–29. https://doi.org/10.1016/j.desal.2016.04.020.
[39] Ortega-Delgado B, García-Rodríguez L, Alarcón-Padilla D-C. Opportunities of improvement of the MED seawater desalination process by pretreatments allowing high-temperature operation. Desalin Water Treat 2017;97:94–108. https://doi.org/10.5004/dwt.2017.21679.
[40] Palenzuela P, Hassan AS, Zaragoza G, Alarcón-Padilla DC. Steady state model for multi-effect distillation case study: Plataforma Solar de Almería MED pilot plant. Desalination 2014;337:31–42. https://doi.org/10.1016/j.desal.2013.12.029.
[41] Palenzuela P, Alarcón-Padilla D-C, Zaragoza G. Concentrating Solar Power and Desalination Plants: Engineering and Economics of Coupling Multi-Effect Distillation and Solar Plants. Springer International Publishing; 2015. doi:10.1007/978-3-319-20535-9.
[42] Lazzaretto A, Tsatsaronis G. SPECO: a systematic and general methodology for calculating efficiencies and costs in thermal systems. Energy 2006;31:1257–89. https://doi.org/10.1016/j.energy.2005.03.011.
[43] Petela R. Exergy of heat radiation. J Heat Transfer 1964;86:187. https://doi.org/10.1115/1.3687092.
[44] Dinçer I, Rosen M. EXERGY: Energy. Environment and Sustainable Development: Elsevier Science; 2012.
[45] Piacentino A. Application of advanced thermodynamics, thermoeconomics and exergy costing to a Multiple Effect Distillation plant: In-depth analysis of cost formation process. Desalination 2015;371:88–103. https://doi.org/10.1016/j.desal.2015.06.008.
[46] Sharqawy MH, Lienhard VJH, Zubair SM. On exergy calculations of seawater with applications in desalination systems. Int J Therm Sci 2011;50:187–96. https://doi.org/10.1016/j.ijthermalsci.2010.09.013.
[47] Sharqawy MH, Zubair SM, Lienhard JH. Second law analysis of reverse osmosis desalination plants: an alternative design using pressure retarded osmosis. Energy 2011;36:6617–26. https://doi.org/10.1016/j.energy.2011.08.056.
[48] Bejan A, Tsatsaronis G, Moran M. Thermal Design and Optimization 1995:560.
[49] Ma Y, Morozyuk T, Liu M, Yan J, Liu J. Optimal integration of recompression supercritical CO 2 Brayton cycle with main compression intercooling in solar power tower system based on exergoeconomic approach. Appl Energy 2019;242:1134–54. https://doi.org/10.1016/j.apenergy.2019.03.155.
[50] Adibhatla S, Kaushik SC. Exergy and thermoeconomic analyses of 500 MWe sub critical thermal power plant with solar aided feed water heating. Appl Therm Eng 2017;123:340–52. https://doi.org/10.1016/j.applthermaleng.2017.05.099.
[51] Xiong J, Zhao H, Zhang C, Zheng C, Luh PB. Thermoeconomic operation optimization of a coal-fired power plant. Energy 2012;42:486–96. https://doi.org/10.1016/j.energy.2012.03.020.
[52] Ameri M, Ahmadi P, Hamidi A. Energy, exergy and exergoecnomic analysis of a steam power plant: A case study. Int J Energy Res 2009;33:499–512. https://doi.org/10.1002/er.1495.
[53] Jorgenson J, Mehos M, Denholm P. Comparing the net cost of CSP-TES to PV deployed with battery storage. AIP Conf. Proc., vol. 1734, SolarPACES 2015, Cape Town: American Institute of Physics; 2016, p. 08003. doi:10.1063/1.4949183.
[54] Dieckmann S, Dersch J, Giuliano S, Puppe M, Lüpfert E, Hennecke K, et al. LCOE reduction potential of parabolic trough and solar tower CSP technology until 2025. AIP Conf Proc 2017:1850. https://doi.org/10.1063/1.4984538.
[55] Aly A, Bernardos A, Fernandez-Peruchena CM, Solvang Jensen S, Pedersen AB. Is Concentrated Solar Power (CSP) a feasible option for Sub-Saharan Africa?: investigating the techno-economic feasibility of CSP in Tanzania. Renew Energy 2019;135:1224–40. https://doi.org/10.1016/j.renene.2018.09.065.
[56] Fu R, Feldman D, Margolis R. U.S. Solar Photovoltaic System Cost Benchmark: Q1 2018. 2018. doi:10.7799/1325002.
[57] Shahabi MP, McHugh A, Anda M, Ho G. Comparative economic and environmental assessments of centralised and decentralised seawater desalination options. Desalination 2015;376:25–34. https://doi.org/10.1016/j.desal.2015.08.012.
[58] Global Sea Temperature. Chile Sea Temperatures n.d. https://www.sea-temperature.org/south-america/chile/ (accessed June 7, 2019).
[59] Kassem A, Al-Haddad K, Komljenovic D. Concentrated solar thermal power in Saudi Arabia: definition and simulation of alternative scenarios. Renew Sustain Energy Rev 2017;80:75–91. https://doi.org/10.1016/j.rser.2017.05.157.
[60] Sharma C, Sharma AK, Mullick SC, Kandpal TC. Cost reduction potential of parabolic trough based concentrating solar power plants in India. Energy Sustain Dev 2018;42:121–8. https://doi.org/10.1016/j.esd.2017.10.003.
[61] Boretti A. Cost and production of solar thermal and solar photovoltaics power plants in the United States. Renew Energy Focus 2018;26:93–9. https://doi.org/10.1016/j.ref.2018.07.002.